TABLE III. Allergen-specific IgG and IgG_4 values in paired CB and MB samples, and BU ratio and correlation between CB- and MB-positive only

	CB (n = 92)		MB (n = 92)		CB/MB-positive only				
IgG positive in:	**n**	**Percent***	**n**	**Percent***	**n**	**Percent†**	**BU ratio‡ (CB BUg/MB BUg ± SD)**	**Correlation between CB and MB (r_s)§**	***P* value**
Food									
α-Casein	34	37.0	34	37.0	32	94.1	0.93 ± 0.30	0.75	<.001
β-Casein	7	7.6	8	8.7	7	87.5	0.88 ± 0.24	0.83	.021
α-Lactoalbumin	1	1.1	1	1.1	1	100	1.12 ± 0.00	NA	
β-Lactoglobulin	6	6.5	7	7.6	5	71.4	1.14 ± 0.44	0.90	.037
Ovalbumin	52	56.5	50	54.3	48	96.0	1.30 ± 0.60	0.80	<.001
Ovomucoid	47	51.1	46	50.0	45	97.8	1.18 ± 0.45	0.90	<.001
Milk	24	26.1	27	29.3	24	88.9	0.92 ± 0.26	0.53	.008
Egg white	52	56.5	52	56.5	49	94.2	1.15 ± 0.35	0.87	<.001
Mean						91.2	1.08 ± 0.38		
Inhalant									
Cedar pollen	0	0.0	1	1.1	0	NA	NA	NA	
Df	19	20.7	23	25.0	19	82.6	0.86 ± 0.20	0.71	.001
Dp	24	26.1	25	27.2	23	92.0	0.88 ± 0.28	0.83	<.001
Mean						87.3	0.87 ± 0.24		

	CB (n = 92)		MB (n = 92)		CB/MB-positive only				
IgG_4 positive in:	**n**	**Percent***	**n**	**Percent***	**n**	**Percent†**	**BU ratio‡ (CB BUg4/MB BUg4 ± SD)**	**Correlation between CB and MB (r_s)§**	***P* value**
Food									
α-Casein	34	37.0	33	35.9	33	100	0.93 ± 0.39	0.89	<.001
β-Casein	13	14.1	15	16.3	13	86.7	0.76 ± 0.27	0.95	<.001
α-Lactoalbumin	17	18.0	16	17.0	16	100	0.90 ± 0.42	0.92	<.001
β-Lactoglobulin	40	43.5	42	45.7	38	90.5	1.07 ± 0.42	0.93	<.001
Ovalbumin	68	73.9	67	72.8	67	100	1.19 ± 0.46	0.91	<.001
Ovomucoid	70	76.1	70	76.1	70	100	1.16 ± 0.48	0.93	<.001
Milk	24	26.1	25	27.2	23	92.0	0.76 ± 0.30	0.94	<.001
Egg white	66	71.7	67	72.8	66	98.5	1.15 ± 0.44	0.94	<.001
Mean						96.0	0.99 ± 0.39		
Inhalant									
Cedar pollen	0	NA	0	NA	0	NA	NA	NA	
Df	0	NA	0	NA	0	NA	NA	NA	
Dp	0	NA	0	NA	0	NA	NA	NA	
Mean									

Df, Dermatophagoides farinae; *Dp, Dermatophagoides pteronyssinus*; *NA*, not available due to lack of positive cases.
*Percentages of allergen-specific IgG- and IgG_4-positive samples.
†Percentages of allergen-specific IgG- and IgG_4-positive samples from MB-positive only.
‡BU ratios (CB BUe/MB BUe, CB BUa/MB BUa).
§Correlation coefficient analyzed Spearman's rank correlation test (r_s, *P* value) of allergen-specific IgE and IgA-positive CB and MB-positive only.

coefficients between CB and MB were not available for allergen-specific IgA against the allergens tested (Table II). Furthermore, the correlation coefficients for allergen-specific IgG_4 against inhalant allergens were not available because allergen-specific BUg4 values were below the detection levels (Tables III and IV). The correlation profiles for allergen-specific IgG and IgG_4 against each allergen between CB and MB are shown in Figs E1 and E2 in this article's Online Repository at www.jacionline.org.

DISCUSSION

We recently developed a new allergen diagnosis microarray with high sensitivity by using DLC-coated chips for profiling allergen-specific IgE, IgA, IgG, and IgG_4 against food and inhalant allergens. The DLC chip allows lowering the limit of detection of allergen-specific IgE in the UniCAP system to further dilution at 4- to 8-fold for each allergen,[15] and the detection limit of allergen-specific IgE in the DLC chip had about 5 times higher sensitivity than that in the UniCAP system in MB and serum of allergic patients. The present study demonstrated a larger difference in the detection sensitivity between the DLC chip and the UniCAP system in CB than in MB (Table I). The reason for the larger difference is not clear at this stage, but a relatively high level of nonspecific IgE in CB may disturb the detection of allergen-specific IgE on the UniCAP system but not on the DLC chip system. The latter immobilizes extremely high-density antigens on the surface of the DLC-coated chip[15] and maintains antigen-antibody reactivity even in the presence of high levels of nonspecific IgE. Our highly sensitive allergen-specific IgE detection system is suitable for the detection of low levels of allergen-specific IgE in CB compared with other previous methods.

The presence of IgE antibodies in CB has been analyzed extensively in the past 20 years since it is important in the design of allergy prevention strategies, particularly allergen avoidance

TABLE IV. Correlation of allergen-specific IgE, IgG, and IgG_4 BU between the 92 paired CB and MB

	Correlation between CB and MB					
	IgE		IgG		IgG_4	
Allergen	r_s	*P* value	r_s	*P* value	r_s	*P* value
Food						
α-Casein	0.69	<.001	0.92	<.001	0.94	<.001
β-Casein	0.70	<.001	0.74	<.001	0.85	<.001
α-Lactoalbumin	0.37	<.001	NA		0.68	<.001
β-Lactoglobulin	0.59	<.001	0.58	<.001	0.97	<.001
Ovalbumin	0.56	<.001	0.93	<.001	0.96	<.001
Ovomucoid	0.94	<.001	0.94	<.001	0.97	<.001
Milk	0.60	<.001	0.91	<.001	0.95	<.001
Egg white	0.53	<.001	0.94	<.001	0.97	<.001
Inhalant						
Cedar pollen	0.30	.004	NA		NA	
Df	0.01	.906	0.83	<.001	NA	
Dp	0.19	.073	0.83	<.001	NA	

Df, Dermatophagoides farinae; *Dp, Dermatophagoides pteronyssinus*; *NA*, not available due to lack of positive cases.

during pregnancy.[1-5,19-22] However, there is conflicting evidence on whether allergen-specific IgE in CB is a reflection of fetal immunity or the result of transfer of maternal IgE to the fetus. The controversy is probably related, at least in part, to the low sensitivity of the methods used for the detection of allergen-specific IgE in CB, and precise allergen-specific IgE profiling patterns against food and inhalant allergens are not available at present. The measurement of the total IgE level in CB is not recommended for allergy risk screening.[6] Furthermore, CB sampling by means of needle puncture of the umbilical vein is essential to avoid MB contamination. To deal with these problems, we collected CB by needle puncture of the umbilical vein and analyzed allergen-specific IgE and other immunoglobulins both in CB/NB and MB by using the newly developed highly sensitive allergen diagnosis DLC chip.

The allergen diagnosis DLC chip detected allergen-specific IgE against more than 1 of the allergens tested in 83.7% of CB from infants analyzed. The rate of detection was higher than those reported previously,[6,11] most likely due to the highly sensitive (Table I) and selective detection of allergen-specific IgE by the DLC chip (Fig 2). The representative data of allergen-specific IgE profiling patterns of CB and NB (Fig 1) showed characteristic patterns that were not identical to those in the paired MB. These results indicated lack of contamination of MB in CB and that IgE in CB is a product of the fetus. If IgE in CB is derived from MB through maternofetal transfer,[11] the allergen-specific profiling pattern of the CB should be similar or identical to that of the MB. The results of the DLC chip of no perfect match of the allergen profiles of CB and MB in the paired 92 samples tested support the conclusion that the allergen-specific IgE identified in CB are of fetal origin.

It has been reported that IgA does not cross the placental barrier and is not produced *in utero* in significant amounts.[23] In contrast, maternal IgG antibodies are transferred to the fetus across the placenta by a specific receptor-mediated mechanism.[24,25] The total IgA levels in CB are commonly used to estimate MB contamination and levels greater than 50 μg/L indicate MB contamination.[11,18] In the present study, the total IgA levels in CB of all our samples were less than 50 μg/mL (range, 1.2-19.4 μg/mL), indicating no or minimal MB contamination. The reliability of the data from the DLC chip was also confirmed by the allergen-specific profiles of IgA, IgG, and IgG_4 (Fig 1): the obvious mismatch of the allergen-specific IgA profile of CB and MB supports no maternofetal transfer of IgA. On the other hand, the similar allergen-specific IgG and IgG_4 profiles in CB and MB provide support for the maternofetal transfer of IgG.

The mean proportion of allergen-specific IgE-positive CB with IgE-positive MB against food allergens was 86.4%, which was about 4 times that with IgE-positive MB against inhalant allergens (20.7%), and their mean allergen-specific IgE BU ratios (CB BUe/MB BUe) for food and inhalant allergens were 1.24 and 0.54, respectively (Table II). These results may provide interpretation for the findings shown in Fig 4 and Table IV of higher levels of allergen-specific IgE (BUe) in CB against food allergens than those against inhalant allergens, and strong and significant correlations between CB and MB for food allergen-specific IgE levels, but weaker correlations for inhalant allergen-specific IgE. These data suggest that maternofetal transfer of food allergens is more frequent and easier than that of inhalant allergens, although previous studies showed crossing of food and inhalant allergens through the placenta in *ex vivo* models.[26,27]

The mechanisms of maternofetal transfer of allergens have been discussed extensively, including fetus allergen-uptake[6] of allergen-IgG complexes through the amniotic fluid by aspiration or permeation through the fetal skin[22,28] and through active transplacental transport.[29] Therefore, the presence of allergen-specific IgG levels in MB and CB may increase the risk of maternofetal allergen transfer and induction of allergen-specific IgE in CB.[30] Furthermore, it has been shown that the fetal immune system can produce IgE antibodies from week 11 of gestation,[13] and thus maternofetal transfer of allergen may trigger allergen-specific IgE production *in utero*. Once these food and inhalant allergens are transferred across the barrier, they may induce allergic sensitization *in utero* under the influence of maternal immune conditions.

In our experiments, however, the mean allergen-specific IgG BU ratios (CB BUg/MB BUg) for food and inhalant allergens were not significantly different at 1.08 and 0.87, respectively (Table III), and allergen-specific IgG levels do not necessarily explain the difference in the levels of IgE (BUe) in CB against food and inhalant allergens. At present, the reasons for the difference in the proportion of allergen-specific IgE-positive CB and the levels of IgE against food and inhalant allergens are not clear. To analyze this difference, further measurements should be conducted of food and inhalant allergen levels in CB and maternal circulation at the time of delivery.

Previous studies reported the presence of low (undetectable) levels of allergen-specific IgE in infant blood during the breast-feeding period at 6 months of age, compared with detectable levels of allergen-specific IgE in CB of some infants.[11,31] This observation might be due to the separation after birth from the source of allergens (ie, amniotic fluid and transplacental transport) and also from the maternal immune system. The findings of sequential appearance of first food-related and later in the preschool age of inhalant allergen-related IgE despite constant environmental exposure to the inhalant allergens by birth is a common knowledge. To study the mechanisms of age-dependent changes in the allergic phenotypes, simultaneous measurements of antigen-specific IgE, IgA, IgG_1, IgG_4, and IgG in serum, nasal secretion, and saliva by the DLC chip as well as measurements of cytokine levels in these samples might be helpful. The present

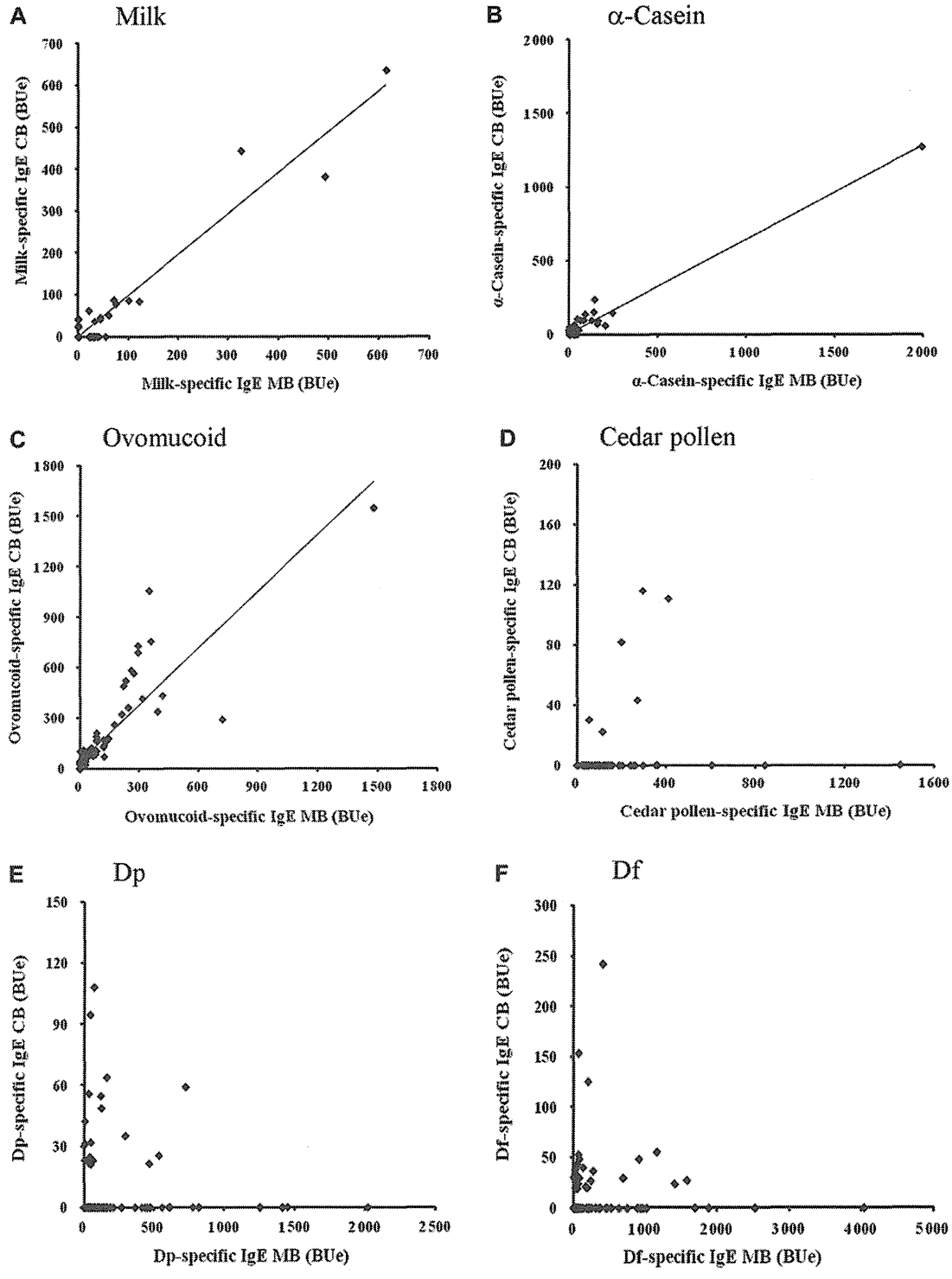

FIG 4. Comparison and correlation of allergen-specific IgE levels between CB and MB analyzed by the DLC chip. Allergen-specific IgE levels in CB and MB (n = 92) depicted in BUe. The cutoff value was 10 BUe. **A,** Milk. **B,** α-Casein. **C,** Ovomucoid. **D,** Cedar pollen. **E,** Dp. **F,** Df. Spearman's rank correlation test was used to assess the relation between the values of CB and MB. *Df, Dermatophagoides farinae; Dp, Dermatophagoides pteronyssinus.*

study found allergen-specific IgG against food and inhalant allergens but no allergen-specific IgG_4 against inhalant allergens in MB and CB. Further studies are also required on the relationship between allergen-specific IgE, IgG, and IgG_4 inductions in fetus and early infantile allergy against food and inhalant allergens.

Conclusions

Analysis using a highly sensitive DLC microarray for allergens demonstrated differences in allergen-specific IgE profiles in 92 paired MB and CB/NB samples. The finding clearly indicates that IgE levels in CB reflect *in utero* sensitization.

We thank all mothers and their babies, as well as the nursing staff, obstetricians, and pediatricians at the Health Insurance Naruto Hospital, JFE Kenpo Kawatetsu Chiba Hospital, and Chiba University Hospital, who participated in this study. We also thank all field workers who were involved in data collection.

Clinical implications: There is evidence for intrauterine sensitization of allergen-specific IgE in cord blood analyzed by a highly sensitive new allergen diagnosis microarray.

REFERENCES

1. Scirica CV, Gold DR, Ryan L, Abulkerim H, Celedon JC, Platts-Mills TA, et al. Predictors of cord blood IgE levels in children at risk for asthma and atopy. J Allergy Clin Immunol 2007;119:81-8.
2. Ege MJ, Herzum I, Büchele G, Krauss-Etschmann S, Lauener RP, Roponen M, et al. Protection Against Allergy Study in Rural Environments (PASTURE) Study group. Prenatal exposure to a farm environment modifies atopic sensitization at birth. J Allergy Clin Immunol 2008;122:407-12.
3. Peters JL, Suglia SF, Platts-Mills TA, Hosen J, Gold DR, Wright RJ. Relationships among prenatal aeroallergen exposure and maternal and cord blood IgE: project ACCESS. J Allergy Clin Immunol 2009;123:1041-6.
4. Halonen M, Stern D, Lyle S, Wright A, Taussig L, Martinez FD. Relationship of total serum IgE levels in cord and 9-month sera of infants. Clin Exp Allergy 1991;21:235-41.
5. Lilja G, Dannaeus A, Falth-Magnusson K, Graff-Lonnevig V, Johansson SG, Kjellman NI, et al. Immune response of the atopic woman and foetus: effects of high- and low-dose food allergen intake during late pregnancy. Clin Allergy 1988;18: 131-42.
6. Pfefferle PI, Sel S, Ege MJ, Büchele G, Blümer N, Krauss-Etschmann S, et al. Cord blood allergen-specific IgE is associated with reduced IFN-γ production by cord blood cells: the Protection against Allergy-Study in Rural Environments (PASTURE) Study. J Allergy Clin Immunol 2008;122:711-6.
7. Nambu M, Shintaku N, Ohta S. Relationship between cord blood level of IgE specific for *Dermatophagoides pteronyssius* and allergic manifestations in infancy. Biol Neonate 2003;83:102-6.
8. Hagendorens MM, Ebo DG, Bridts CH, Van de Walter L, De Clerck LS, Stevens WJ. Prenatal exposure to house dust mite allergen (Der p 1), cord blood T cell phenotype and cytokine production and atopic dermatitis during the first year of life. Pediatr Allergy Immunol 2004;15:308-15.
9. Piastra M, Stabile A, Fioravanti G, Castagnola M, Pani G, Ria F. Cord blood mononuclear cell responsiveness to beta-lactoglobulin: T-cell activity in "atopy-prone" and "non-atopy-prone" newborns. Int Arch Allergy Immunol 1994;104:358-65.
10. Prescott SL, Macaubas C, Smallacombe T, Holt BJ, Sly PD, Holt PG. Development of allergen-specific T-cell memory in atopic and normal children. Lancet 1999;353: 196-200.
11. Bønnelykke K, Pipper CB, Bisgaard H. Transfer of maternal IgE can be a common cause of increased IgE levels in cord blood. J Allergy Clin Immunol 2010;126: 657-63.
12. Rowe J, Kusel M, Holt BJ, Suriyaarachchi D, Serralha M, Hollams E, et al. Prenatal versus postnatal sensitization to environmental allergens in a high-risk birth cohort. J Allergy Clin Immunol 2007;119:1164-73.
13. Miller DL, Hiravonen T, Gitlin D. Synthesis of IgE by the human conceptus. J Allergy Clin Immunol 1973;52:182-8.
14. Lima JO, Zhang L, Atkinson TP, Philips J, Dasanayake AP, Schroeder HW Jr. Early expression of iepsilon, CD23 (FcepsilonRII), IL-4Ralpha, and IgE in the human fetus. J Allergy Clin Immunol 2000;106:911-7.
15. Suzuki K, Hiyoshi M, Tada H, Bando M, Ichioka T, Kamenura N, et al. Allergen diagnosis microarray with high-density immobilization capacity using diamond-like carbon-coated chips for profiling allergen-specific IgE and other immunoglobulins. Anal Chim Acta 2011;706:321-7.
16. Ewan PW, Coote D. Evaluation of a capsulated hydrophilic carrier polymer (the ImmunoCAP) for measurement of specific IgE antibodies. Allergy 1990;45: 22-9.
17. Simister NE. Placental transport of immunoglobulin G. Vaccine 2003;21:3365-9.
18. Ownby DR, McCullough J, Johnson CC, Peterson EL. Evaluation of IgA measurements as a method for detecting maternal blood contamination of cord blood samples. Pediatr Allergy Immunol 1996;7:125-9.
19. Heinrich J, Bolte G, Holscher B, Douwes J, Lehmann I, Fahlbusch B, et al. Allergens and endotoxin on mothers' mattresses and total immunoglobulin E in cord blood of neonates. Eur Respir J 2002;20:617-23.
20. Karmaus W, Arshad H, Mattes J. Does the sibling effect have its origin in utero? Investigating birth order, cord blood immunoglobulin E concentration, and allergic sensitization at age 4 years. Am J Epidemiol 2001;154:909-15.
21. Sadeghnejad A, Karmaus W, Davis S, Kurukulaaratchy RJ, Matthews S, Arshad SH. Raised cord serum immunoglobulin E increases the risk of allergen sensitization at ages 4 and 10 and asthma at age 10. Thorax 2004;59:936-42.
22. Vance GHS, Lewis SA, Grimshaw KEC, Wood PJ, Briggs RA, Thornton CA, et al. Exposure of the fetus and infant to hens' egg ovalbumin via the placenta and breast milk in relation to maternal intake of dietary egg. Clin Exp Allergy 2005;35: 1318-26.
23. Malek A, Sager R, Kuhn P, Nicolaides KH, Schneider H. Evolution of maternofetal transport of immunoglobulins during human pregnancy. Am J Reprod Immunol 1996;36:248-55.
24. Saji F, Samejima Y, Kamiura S, Koyama M. Dynamics of immunoglobulins at the feto-maternal interface. Rev Reprod 1999;4:81-9.
25. Jenmalm MC, Björkstén B. Cord blood levels of immunoglobulin G subclass antibodies to food and inhalant allergens in relation to maternal atopy and the development of atopic disease during the first 8 years of life. Clin Exp Allergy 2000;30: 34-40.
26. Loibichler C, Pichler J, Gerstmayr M, Bohle B, Kiss H, Urbanek R, et al. Maternofetal passage of nutritive and inhalant allergens across placentas of term and preterm deliveries perfused *in vitro*. Clin Exp Allergy 2001;32:1546-51.
27. Szépfalusi Z, Loibichler C, Hänel-Dekan S, Dehlink E, Gerstmayr M, Pichler J, et al. Most of diaplacentally transferred allergen is retained in the placenta. Clin Exp Allergy 2006;36:1130-7.
28. Holloway JA, Warner JO, Vance GH, Diaper ND, Warner JA, Jones CA. Detection of house-dust-mite allergen in amniotic fluid and umbilical-cord blood. Lancet 2000;356:1900-2.
29. Avrech OM, Samra Z, Lazarovich Z, Caspi E, Jacobovich A, Sompolinsky D. Efficacy of the placental barrier for immunoglobulins: correlations between maternal, paternal and fetal immunoglobulin levels. Int Arch Allergy Immunol 1994;103: 160-5.
30. Eysink PE, De Jong MH, Bindels PJ, Scharp-Van Der Linden VT, De Groot CJ, Stapel SO, et al. Relation between IgG antibodies to foods and IgE antibodies to milk, egg, cat, dog and/or mite in a cross-sectional study. Clin Exp Allergy 1999;29:604-10.
31. Bønnelykke K, Pipper CB, Bisgaard H. Sensitization does not develop *in utero*. J Allergy Clin Immunol 2008;121:646-51.

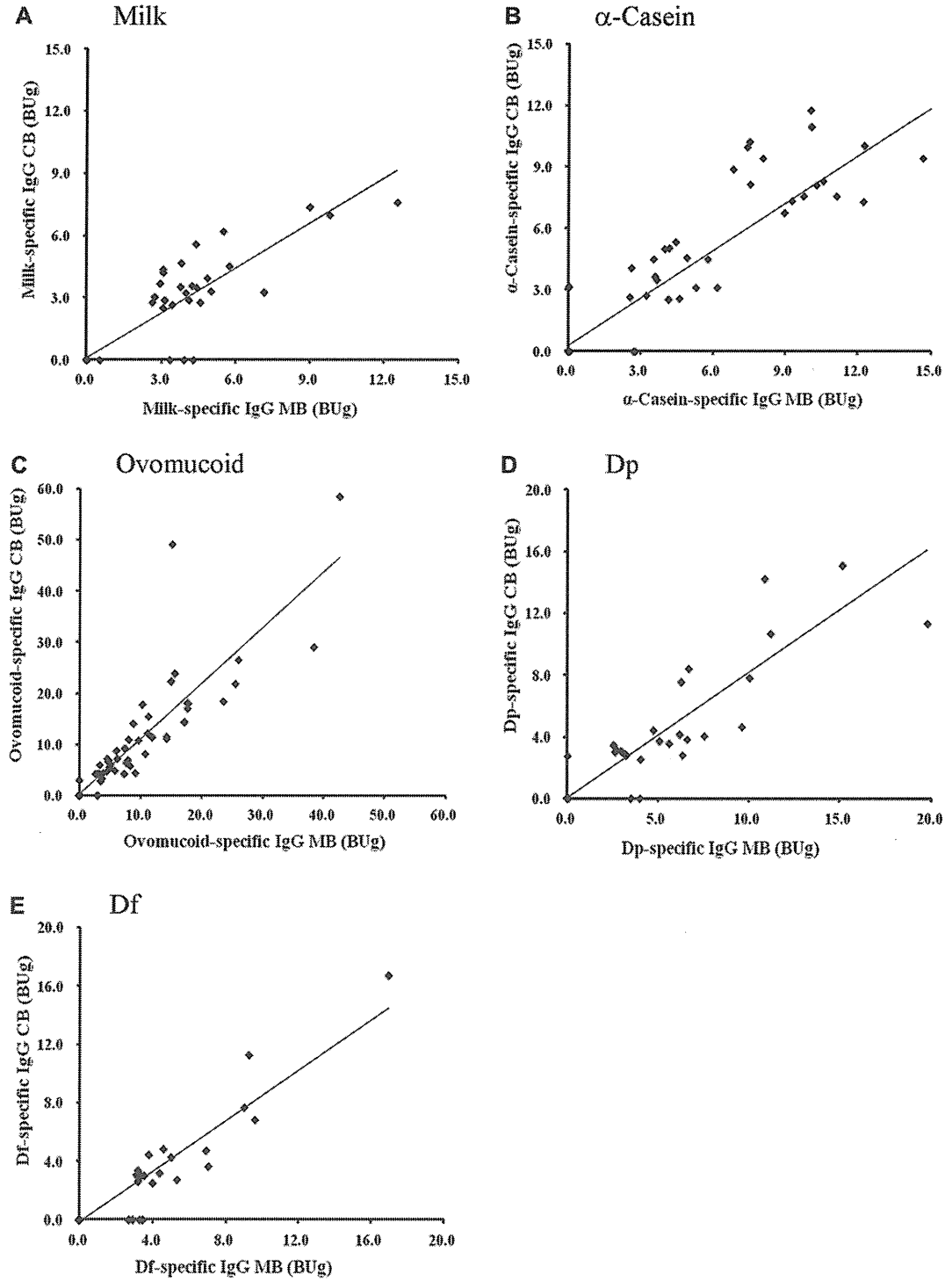

FIG E1. Comparison of allergen-specific IgG levels in CB and MB analyzed by the DLC chip. Allergen-specific IgG levels in paired samples of CB and MB (n = 92) depicted in BUg. The cutoff value was 2.50 BUg. **A,** Milk. **B,** α-Casein. **C,** Ovomucoid. **D,** Dp. **E,** Df. Spearman's rank correlation test was used to assess the relation between CB and MB. *Df, Dermatophagoides farinae; Dp, Dermatophagoides pteronyssinus.*

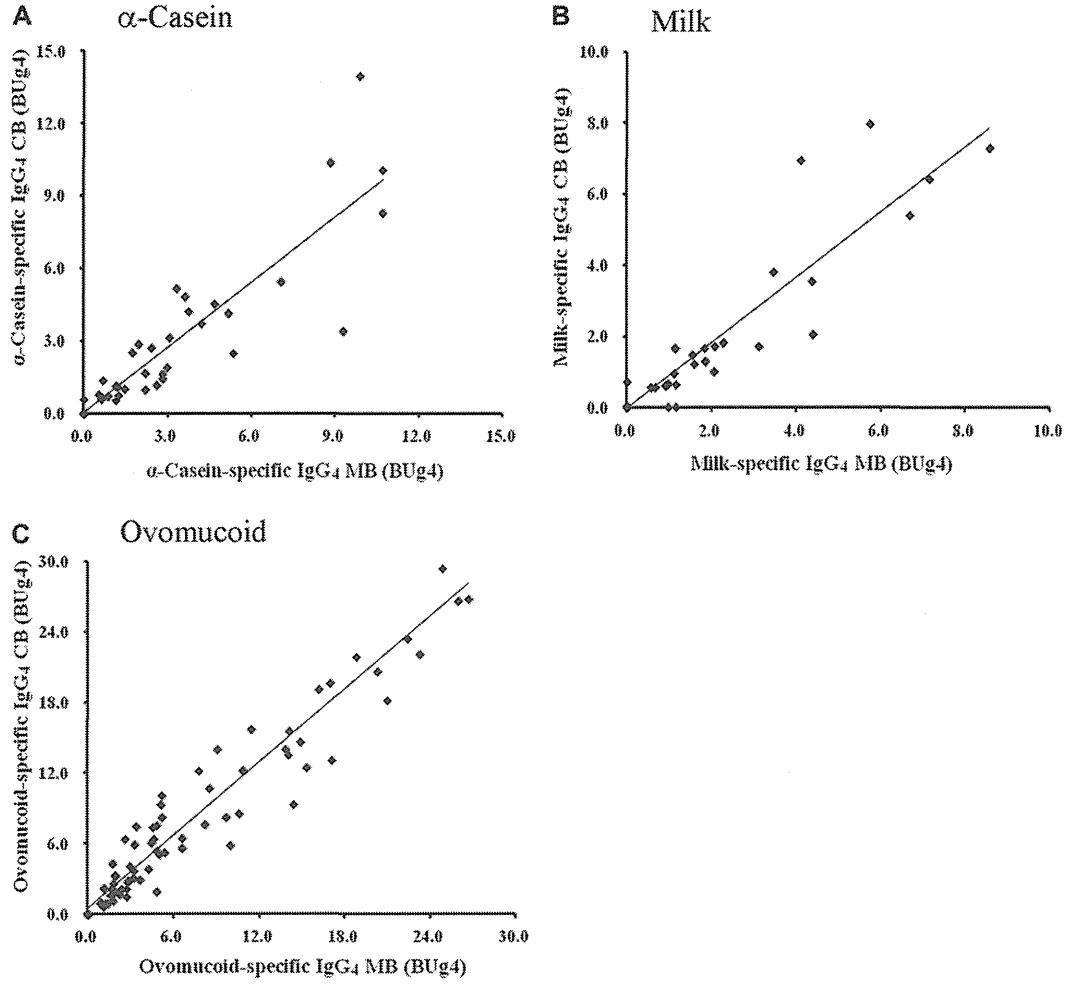

FIG E2. Comparison of allergen-specific IgG_4 levels in CB and MB analyzed by the DLC chip. Allergen-specific IgG_4 levels in paired samples of CB and MB (n = 92) depicted in BUg4. The cutoff value was 0.53 BUg4. **A,** α-Casein. **B,** Milk. **C,** Ovomucoid. Spearman's rank correlation test was used to assess the relation between CB and MB.

Characterization of dsRNA-induced pancreatitis model reveals the regulatory role of *IFN regulatory factor 2* (*Irf2*) in *trypsinogen5* gene transcription

Hideki Hayashi[a], Tomoko Kohno[a], Kiyoshi Yasui[a], Hiroyuki Murota[b], Tohru Kimura[c], Gordon S. Duncan[d], Tomoki Nakashima[e], Kazuo Yamamoto[d], Ichiro Katayama[b], Yuhua Ma[a], Koon Jiew Chua[a], Takashi Suematsu[a], Isao Shimokawa[f], Shizuo Akira[g], Yoshinao Kubo[a], Tak Wah Mak[d,1], and Toshifumi Matsuyama[a,h,1]

[a]Division of Cytokine Signaling, Department of Molecular Biology and Immunology and [f]Department of Investigative Pathology, Nagasaki University Graduate School of Biomedical Science, Nagasaki 852-8523, Japan; Departments of [b]Dermatology and [c]Pathology, Graduate School of Medicine and [g]Department of Host Defense, Research Institute for Microbial Diseases, Osaka University, Osaka 565-0871, Japan; [d]Campbell Family Cancer Research Institute, Princess Margaret Hospital, Toronto, ON, Canada M5G 2M9; [e]Department of Cell Signaling, Tokyo Medical and Dental University, Tokyo 113-8549, Japan; and [h]Global Center of Excellence Program, Nagasaki University, Nagasaki 852-8523, Japan

Contributed by Tak Wah Mak, October 5, 2011 (sent for review September 8, 2011)

Mice deficient for *interferon regulatory factor* (*Irf*)*2* (*Irf2*$^{-/-}$ mice) exhibit immunological abnormalities and cannot survive lymphocytic choriomeningitis virus infection. The pancreas of these animals is highly inflamed, a phenotype replicated by treatment with poly(I:C), a synthetic double-stranded RNA. Trypsinogen5 mRNA was constitutively up-regulated about 1,000-fold in *Irf2*$^{-/-}$ mice compared with controls as assessed by quantitative RT-PCR. Further knockout of *IFNα/β receptor 1* (*Ifnar1*) abolished poly(I:C)-induced pancreatitis but had no effect on the constitutive up-regulation of *trypsinogen5* gene, indicating crucial type I IFN signaling to elicit the inflammation. Analysis of *Ifnar1*$^{-/-}$ mice confirmed type I IFN-dependent transcriptional activation of dsRNA-sensing pattern recognition receptor genes *MDA5*, *RIG-I*, and *TLR3*, which induced poly(I:C)-dependent cell death in acinar cells in the absence of IRF2. We speculate that Trypsin5, the *trypsinogen5* gene product, leaking from dead acinar cells triggers a chain reaction leading to lethal pancreatitis in *Irf2*$^{-/-}$ mice because it is resistant to a major endogenous trypsin inhibitor, Spink3.

TRIF | IPS-1 | Ca^{2+}-binding proteins | cathepsin B

Interferons (IFNs) are cytokines whose actions contribute to the first line of defense against infection. IFNs both render cells resistant to viral attack and regulate cell growth and differentiation (1). IFNs elicit their pleiotropic effects by regulating the expression of many IFN-stimulated genes (ISGs). IFNs themselves are controlled by IFN regulatory factors (IRFs) that also regulate the expression of ISGs. By binding to IFN-stimulated response elements (ISREs) in gene promoters, the nine known IRF family members (IRF1–9) govern the production of cytokines related to inflammation and immune responses.

When pattern recognition receptors (PRRs) such as Toll-like receptors (TLRs) and retinoic acid-inducible gene-I (RIG)-like receptors detect pathogen ligands, these receptors are activated (2) and transduce downstream signaling, activating IRFs and IFNs. Analyses using knockout (KO) mice deficient for various IRFs have revealed their physiological roles. For example, IRF2 functions mainly as a transcriptional repressor by competing for binding to ISREs with other IRFs, especially IRF9 and IRF1 (1).

Irf2-deficient (*Irf2*$^{-/-}$) mice spontaneously develop inflammatory skin disease as they age, and die within weeks from lymphocytic choriomeningitis virus (LCMV) infection (3). Ablation of *IFNα/β receptor 1* (*Ifnar1*) or *Irf9* ameliorates the skin inflammation of *Irf2*$^{-/-}$ mice, suggesting that IRF2 negatively regulates gene expression by antagonizing IRF9, which is activated by type I IFN (I-IFN) (4). However, the precise mechanisms underlying the phenotypes of *Irf2*$^{-/-}$ are not known. In this study, we found that poly(I:C) (pIC) mimicked LCMV-induced pancreatitis, and we have used double KO mice to explore the cause of death in pIC-treated *Irf2*$^{-/-}$ mice. Our results show that significant trypsinogen5 up-regulation in *Irf2*$^{-/-}$ mice together with I-IFN-dependent transcriptional activation of dsRNA-sensing PRRs were critical for the pIC-induced death.

Results and Discussion

***Irf2*$^{-/-}$ Mice Show IFN-Dependent Poly(I:C)-Induced Pancreatitis and IFN-Independent Secretory Dysfunction in Pancreatic Acinar Cells.** LCMV-infected *Irf2*$^{-/-}$ mice die within 4 wk postinfection (3), but all *Irf2*$^{-/-}$ mice challenged intraperitoneally with poly(I:C) (pIC-*Irf2*$^{-/-}$ mice) died within 1 wk (Fig. 1*A*). Severe acute pancreatitis was apparent in pIC-*Irf2*$^{-/-}$ mice, as shown by abundant TUNEL^{+} apoptotic cells (Fig. 1*B*). Even in the absence of pIC, however, some abnormalities were detected in *Irf2*$^{-/-}$ pancreas, as indicated by hematoxylin and eosin staining (Fig. 1*C*) and electron microscopy (Fig. 1*D*). A mild infiltration of inflammatory cells (particularly lymphocytes) was noted around *Irf2*$^{-/-}$ ductal cells, but this pancreatitis was not typical. The pancreatic acinar cells in untreated *Irf2*$^{-/-}$ mice were filled with eosinophilic secretory granules of heterogeneous size, whereas fewer eosinophilic granules of more uniform size were observed mainly in the apical region of WT acinar cells. Interestingly, treatment of *Irf2*$^{-/-}$ mice with the stable cholecystokinin (CCK) analog cerulein (5) did not cause acute pancreatitis, as assessed by electron microscopy and serum amylase levels (Fig. S1 *A* and *B*). Because mRNA expression of CCK receptors in *Irf2*$^{-/-}$ mice was normal (Fig. S1*C*), these results suggest that the secretory and/or vesicle transport systems in *Irf2*$^{-/-}$ mice are dysfunctional.

The mRNAs encoding the Ca^{2+}-binding proteins Anxa10, Ahsg, and S100-G involved in Ca^{2+}-dependent vesicle transport, sorting, and fusion processes were significantly up-regulated in *Irf2*$^{-/-}$ pancreas (Table S1). The secretory dysfunction observed in cerulein-treated *Irf2*$^{-/-}$ mice (6), which is due to an abnormal distribution pattern of normal levels of soluble *N*-ethylmaleimide-sensitive factor attachment protein receptors (SNAREs) (6), may be due to the abnormal expression of these Ca^{2+}-binding proteins in the absence of IRF2, because annexin family proteins are known to bind and regulate SNAREs (7).

Skin inflammation in *Irf2*$^{-/-}$ mice was rescued by abolishing IFN signaling (4). We asked whether the atypical pancreatitis in *Irf2*$^{-/-}$ mice could be similarly rescued by crossing the *Irf2*$^{-/-}$ mutants to *Ifnar1*-, *Irf1*-, or *Trif*-deficient mice (3, 8, 9) to gen-

Author contributions: H.H., T. Kohno, I.K., T.W.M., and T.M. designed research; H.H., T. Kohno, K. Yasui, H.M., T. Kimura, G.S.D., T.N., K. Yamamoto, Y.M., K.J.C., T.S., and T.M. performed research; T. Kimura, I.S., and S.A. contributed new reagents/analytic tools; Y.K. and T.W.M. analyzed data; and H.H. and T.M. wrote the paper.

The authors declare no conflict of interest.

Freely available online through the PNAS open access option.

[1]To whom correspondence may be addressed. E-mail: tmak@uhnres.utoronto.ca or tosim@nagasaki-u.ac.jp.

This article contains supporting information online at www.pnas.org/lookup/suppl/doi:10.1073/pnas.1116273108/-/DCSupplemental.

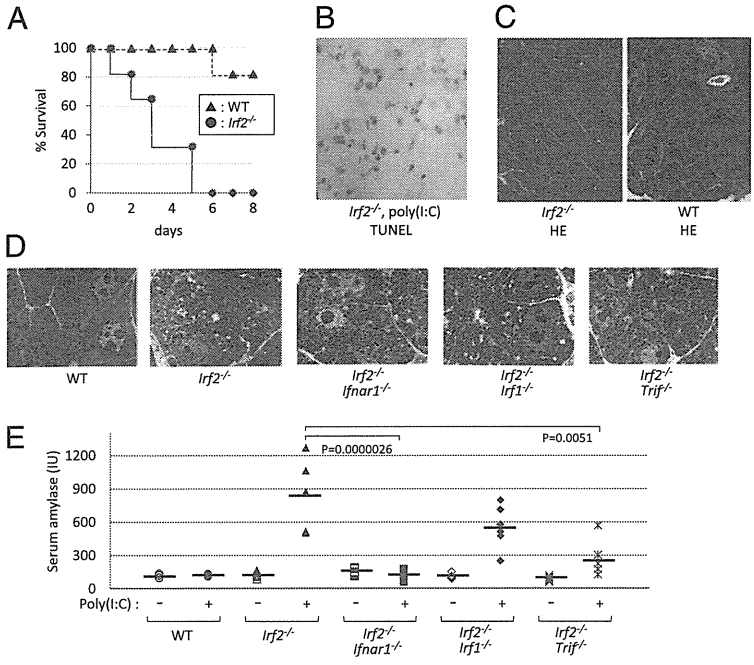

Fig. 1. *Irf2* deficiency induces sensitivity to poly(I:C) and pancreatitis. (*A*) Survival curve after pIC challenge. WT and *Irf2*-deficient ($Irf2^{-/-}$) mice were induced by i.p. pIC challenge (250 μg). All of the $Irf2^{-/-}$ mice were deceased within a week, compared with WT mice. (*B*) Following pIC stimulation, many cells were TUNEL-positive, indicating apoptosis and severe acute pancreatitis in $Irf2^{-/-}$ mice. (*C* and *D*) Hematoxylin and eosin (HE) staining (*C*) and electron microscopic observation (*D*) were done to examine the pancreas histologically in WT, $Irf2^{-/-}$, and double KO mice ($Irf2^{-/-}Ifnar1^{-/-}$, $Irf2^{-/-}Irf1^{-/-}$, and $Irf2^{-/-}Trif^{-/-}$). (*E*) To assess pancreatitis, we monitored serum amylase levels with (+) and without (–) pIC challenge.

erate double knockout mice. Abnormal acinar granule distribution was again observed in $Irf2^{-/-}Ifnar1^{-/-}$, $Irf2^{-/-}Irf1^{-/-}$, and $Irf2^{-/-}Trif^{-/-}$ mice (Fig. 1*D*). Thus, the abnormal acinar structure caused by *Irf2* disruption is not mediated by IFN signaling.

To assess pancreatitis in double knockout mice, we measured serum amylase levels before and after pIC challenge (Fig. 1*E*). Serum amylase was elevated in pIC-$Irf2^{-/-}$ and pIC-$Irf2^{-/-}Irf1^{-/-}$ mice. However, this increase did not occur at all in pIC-$Irf2^{-/-}Ifnar1^{-/-}$ mice, and only to a limited extent in pIC-IRF2$^{-/-}$TRIF$^{-/-}$ mice. These data indicate that type I IFN signaling via IFNAR1, as well as TLR signaling via the adaptor protein TRIF, are important for the development of pIC-induced pancreatitis in $Irf2^{-/-}$ mice. Moreover, our results show that IRF2 regulates IFN-independent pathways affecting acinar cell secretion as well as IFN-dependent pathways inducing pIC-mediated pancreatitis.

Up-Regulated Trypsinogen5 mRNA in the Pancreas of $Irf2^{-/-}$ Mice. We used an Affymetrix DNA microarray system to compare mRNA expression in the pancreas before and after pIC injection of $Irf2^{-/-}$ and WT mice (Fig. 2*A*). In $Irf2^{-/-}$ mice, 14 annotated genes were up-regulated and 8 genes were down-regulated more than 10-fold (Table S1) compared with WT mice. The transcriptional profiles of genes important for the etiology of pancreatitis (10, 11) are listed in Table 1. Strikingly, trypsinogen5 mRNA was up-regulated >100-fold in pIC-$Irf2^{-/-}$ pancreas, a noteworthy observation because trypsinogens activate many other pancreatic enzymes, and premature intracellular activation of trypsinogens in pancreatic acinar cells triggers acute pancreatitis (10, 11). There are 20 *trypsinogen* genes (*T1–T20*) in the murine T-cell receptor β gene locus (12), 12 of which express trypsinogen proteins (Fig. S2, *Right*), whereas humans have only 3 *trypsinogen* genes encoding three proteins: PRSS1, PRSS2, and PRSS3 (Fig. S2, *Left*) (13). The gene expression profile of pIC-$Irf2^{-/-}$ pancreas is inflammation-prone: Mouse trypsinogen mRNAs of T11 (Prss3) and T4 (Trypsinogen5) were up-regulated (Table 1); the mRNA encoding cysteine protease cathepsin B (Ctsb), an enzyme that can initiate pancreatitis by activating trypsinogens (14–16), was also up-regulated (Table 1). The mRNA encoding chymotrypsin C (Ctrc) was down-regulated and another anti-inflammatory factor inter-α-trypsin inhibitor was also down-regulated, although the mRNA encoding Kazal type 3 (Spink3), a serine protease inhibitor that blocks trypsin activity (17), was slightly up-regulated.

We examined the tissue specificity and dependency on IRF2 and IFNAR1 of trypsinogen5 expression by quantitative RT-PCR. In untreated WT mice, trypsinogen5 is expressed most highly in pancreas and skin and modestly in spleen (Fig. S3*A*). In untreated $Irf2^{-/-}$ mice, trypsinogen5 expression in the pancreas was up-regulated ~1,000-fold compared with controls, and was not affected by IFNAR1 ablation. Trypsinogen5 mRNA was up-regulated in $Irf2^{-/-}$ spleen to a much lower extent than in $Irf2^{-/-}$ pancreas, and was not detectable in liver or lung of WT or $Irf2^{-/-}$ mice.

We examined the effects of various IRFs on the activity of the murine *trypsinogen5* promoter, which contains seven ISREs. We cloned a 1.1-kb fragment of the *trypsinogen5* promoter region (−1063 to +15) to create a series of promoter deletion construct mutants driving the firefly luciferase reporter gene (Fig. 2*B*, *Left*). These were transfected into HEK293T cells along with plasmids overexpressing murine IRF1, human IRF5, IRF7, or MyD88. MyD88 was required for IRF-mediated activation of *trypsinogen5* ISREs, and significant promoter activity was observed when IRF1, IRF5, or IRF7 was overexpressed (Fig. S3*B*). Furthermore, the −216 to +15 promoter region of *trypsinogen5* was sufficient for responses to IRF1 or IRF7 stimulation (Fig. S3*C*). Overexpression of IRF2 inhibited IRF1- or IRF7-stimulated promoter activity in a dose-dependent manner (Fig. S3*D*). These data suggest that IRF2 binds to the proximal promoter of *trypsinogen5* and inhibits the access of IRF1, IRF5, and IRF7 to ISRE sites in this region.

To confirm this hypothesis, we transfected TGP49 cells, a mouse acinar cell line, with *trypsinogen5* promoter deletion series reporters as well as with plasmids expressing IRF1, -5, or -7, and assessed the promoter activities (Fig. 2*B*, *Right*). The basal promoter activity was drastically decreased by deleting the −216 to −100 region containing two ISREs, a nuclear factor-activated T cell (NFAT), and an activator protein 1 (AP-1) binding site. In contrast to 293T cells, the *trypsinogen5* promoter in TGP49 cells could be activated by exogenously expressed IRF5 or IRF7 without MyD88 (Fig. 3*A*). The promoter could not be activated by IRF1 even in the presence of MyD88 expression. The regions responsive to IRF5 and IRF7 were confirmed to be ISRE4 (−62 to −59) and ISRE3 (−55 to −49) by site-specific mutation analysis (Fig. 2*C*). The IRF5- and IRF7-dependent promoter activities were significantly ($P < 0.05$) enhanced by knocking down Irf2 with specific siRNA compared with control (scrambled) siRNA (Fig. 3*A*).

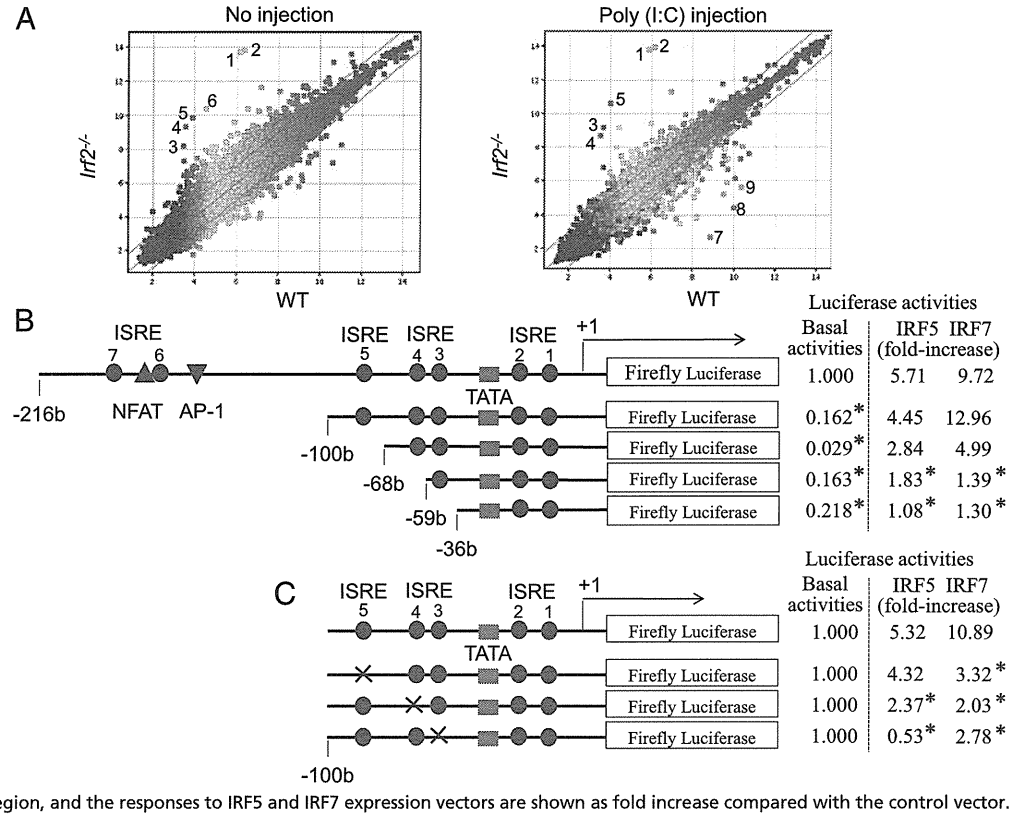

Fig. 2. Trypsinogen5 is highly expressed in *Irf2*-deficent mice. (*A*) *Irf2*$^{-/-}$ or wild-type mice with or without peritoneal injection of pIC were killed, and the amounts of mRNA from the pancreas were systematically compared using Affymetrix 28,815 gene probes. The points farthest from the diagonal indicate transcripts showing the greatest difference between WT and *Irf2*$^{-/-}$. Points 1 and 2, trypsinogen5 with different probes; 3, α-2-HS-glycoprotein (Ahsg); 4, annexin A10 (Anxa10); 5, fetuin-β (Fetub); 6, 3-hydroxy-3-methylglutaryl-Coenzyme A synthase2 (Hmgcs2, HMG-CoA synthase); 7, Ig κ chain variable8 (Igk-V8); 8, unknown; 9, carbonic anhydrase 3 (Car3). (*B*) A series of deletion mutants of *trypsinogen5* proximal promoter region (−216 to +15) was placed upstream of a luciferase reporter gene (1 μg) and analyzed for transcriptional activity in mouse pancreatic acinar cells using a dual luciferase assay at 24 h posttransfection in combination with expression vectors (100 ng) expressing IRF5 or IRF7 or a control vector. The basal luciferase activity of each deletion, measured relative to the −216 to +15 region, and the responses to IRF5 and IRF7 expression vectors are shown as fold increase compared with the control vector. The TATA box, ISRE core, and NFAT- and AP-1 binding sites are indicated. *$P < 0.05$ versus the −216 to +15 region. (*C*) Point mutations were introduced into each ISRE site (indicated by x) of the *trypsinogen5* promoters as described in *Materials and Methods*. The promoter activity of each mutant *trypsinogen5* was determined with a dual luciferase assay system. *$P < 0.05$ versus wild type.

To confirm IRF2 binding to the proximal promoter of trypsinogen5 in pancreatic acinar cells in vivo, we performed chromatin immunoprecipitation (ChIP) assays in TGP49 cells using specific PCR probes spanning all seven ISREs (−173 to +56) in the *trypsinogen5* promoter. Anti-IRF2 antibody specifically precipitated the *trypsinogen5* promoter, as determined by semi-quantitative PCR (Fig. 3*B*) and real-time PCR (Fig. 3*C*). These results suggest that in WT mice, trypsinogen5 expression in pancreatic acinar cells is repressed by the binding of IRF2 to ISREs in the proximal promoter region. However, in *Irf2*$^{-/-}$ mice, the *trypsinogen5* gene is activated because IRF5 and IRF7 can access the ISREs in the absence of IRF2.

IRF5 and IRF7 are critical inducers of the expression of proinflammatory cytokines and type I IFNs, respectively (18, 19), and these activities require MyD88. In WT cells, IRF4 inhibits IRF5 function by sequestering MyD88 (18). IRF2 did not associate with MyD88 (18) but, in our study, it did bind to the ISRE-containing region in the trypsinogen5 promoter (Fig. 3 *B* and *C*). Therefore, we postulate that IRF2 inhibits IRF5 and IRF7 activity by competing with them for binding to ISREs, rather than by sequestering MyD88.

Trypsinogen5 Is Resistant to the Trypsin Inhibitor Spink3. Comparison of mouse trypsinogen5 to other mouse and human trypsinogens (Fig. S4) showed that, although the N-terminal activation peptide sequence (NSDDK-I) in trypsinogen5 differs from that in other trypsinogens (DDDDK-I), other important regions, including the triad amino acid sequence H-D-S, required for enzymatic activity are conserved (10, 11). In addition, tryptic activity in cell lysates of 293FT cells overexpressing trypsinogen5 was dramatically enhanced by treatment with enteropeptidase (Fig. 4 *A* and *B*). The trypsinogen5 inhibitor binding site (DSCDGDS), which prevents premature activation, differed from that found in most trypsinogens (DSCQGDS) (10, 11), resembling the inhibitor binding site (DSCQRDS) of the human trypsin inhibitor-resistant PRSS3 enzyme. In addition, the trypsin autolytic cleavage site (Q-V) in trypsinogen5 differed from that in other trypsinogens (R-V), suggesting that trypsinogen5 is resistant to both trypsin inhibitors and self-inactivation. Indeed, trypsinogen5 was resistant to inhibition by Spink3, a major en-

Table 1. Expressions of relevant genes to pancreatitis

Gene transcripts	WT (–)	WT (pIC)	*Irf2*$^{-/-}$ (–)	*Irf2*$^{-/-}$ (pIC)
Prss1 (T16, Trypsin1)	11,161	13,863	10,388	13,788
Prss2 (T20, Trypsin 2)	16,041	15,661	15,857	15,494
Prss3 (T11, Trypsin 3)	1,155	1,131	3,059 ↑	2,395 ↑
Trypsinogen5 (T4, 1810009J06Rik)	70	57	13,514 ↑	14,287 ↑
Chymotrypsin C (Ctrc)	545	368	87 ↓	119 ↓
Chymotrypsinogen B 1 (Ctrb1)	19,417	18,772	20,457	19,919
Amylase2-2, pancreatic (Amy2b)	19,101	18,488	17,092	18,261
Calcium-sensing receptor (Casr)	37	37	30	26
Cystic fibrosis membrane conductance regulator (Cftr)	7	6	11	8
Cathepsin B (Ctsb)	349	443	848 ↑	794 ↑
Serine protease inhibitor, Kazal-type 3 (Spink3)	4,716	3,957	7,497	7,774
Inter-α-trypsin inhibitor, heavy chain 4 (Itih4)	375	212	78 ↓	71 ↓
Galanin (Gal)	879	1,057	213 ↓	71 ↓

The levels of gene expression in the pancreas are shown in Affymetrix units. The trypsinogen5 data are Point 1 in Fig. 2.

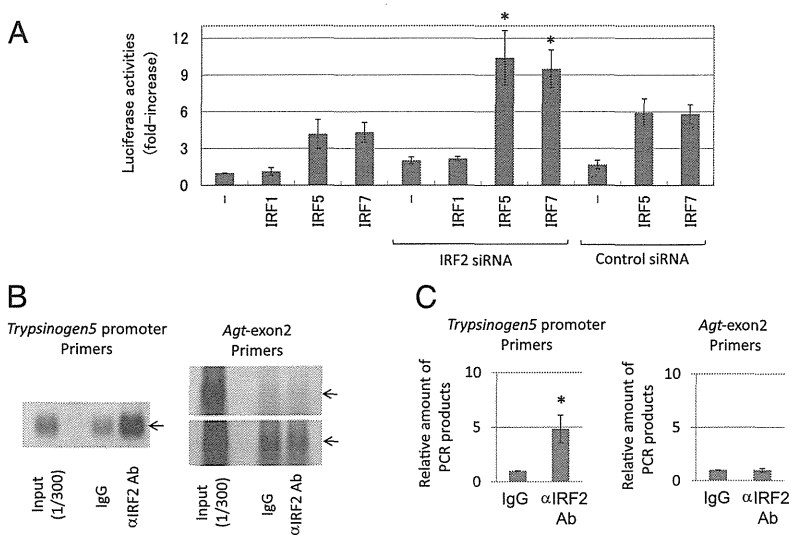

Fig. 3. IRF2 binds to the promoter region of *trypsinogen5* gene. (*A*) The effects of siRNAs (3 μg) specific to IRF2 or a control scrambled sequence on transcriptional activity of the −216 to +15 luciferase reporter in TGP49 acinar cells were measured. **P* < 0.05 versus control siRNA. (*B*) A chromatin immunoprecipitation assay was done using TGP49 acinar cells with the IRF2-specific antibody (5 μg) or the same amount of control nonspecific IgG. The precipitated chromatin fragments were detected by PCR with a *trypsinogen5* promoter-specific primer set at 35 cycles or a negative control primer set for *angiotensinogen* (*Agt*) exon2 at 30 (*Upper*) and 35 (*Lower*) cycles. The input before precipitation indicates the predicted size (Trp5, 229 bp; Agt, 221 bp) of the PCR product. (*C*) The ChIP assay done in *B* was quantitatively measured using a real-time PCR method with the same primers. The relative amounts of β-actin were calculated, and the amounts of chromatin fragments precipitated with the anti-IRF2 antibody were shown relative to those with the nonspecific control antibody (IgG). **P* < 0.01 versus control IgG.

dogenous trypsin inhibitor in mice (Fig. 4 *C* and *D*), as well as by soy bean trypsin inhibitor (Fig. S5 *A* and *B*). Analysis of the evolutionary pedigree in Fig. S6 showed that mouse trypsinogen5 is most distant from mPrss1 and mPrss2, just as human PRSS3 is most distant from PRSS1 and PRSS2. Therefore, we believe that mouse trypsinogen5 is a homolog of human PRSS3. Moreover, our data suggest that, in the absence of IRF2, trypsinogen5 is highly expressed and exacerbates pIC-induced pancreatitis due to its inhibitor-resistant nature.

Poly(I:C)-Induced Cell Death Can Be Triggered by a TLR3/TRIF-Dependent Pathway or a RIG-I/MDA5/IPS-1-Dependent Pathway. Although trypsinogen5 was up-regulated in untreated IRF2$^{-/-}$ mice, only mild inflammation around acinar cells was observed and pancreatitis did not occur. We hypothesize that trypsinogen5 as well as mPrss1, -2, and -3 leaking from dying acinar cells are activated by proteases such as cathepsin B or enteropeptidase, also released from these cells. These activated trypsins trigger signals to induce the death of many acinar cells, a process of cell death amplification we refer to as the "enhancing loop" of acinar cell death. In this way, the initial death of a few cells induced by pIC can precipitate severe pancreatitis. This idea is supported by a report that the extracellular or intracellular treatment of pancreatic acinar cells with active trypsins causes acinar cell death (20). In this study, the enteropeptidase cleavage site (-DDDDK-) of rat trypsinogen was replaced with a cleavage site (-RTKR-) recognized by paired basic amino acid-cleaving enzyme (PACE). This allowed the rat trypsinogen to be activated intracellularly with the ubiquitously expressed PACE enzyme rather than with enteropeptidase, which is expressed mainly in the duodenum. We created a PACE-trypsinogen5 enzyme that successfully induced the apoptosis of 293FT cells when overexpressed (Fig. 4 *E* and *F*). These results indicate that proteolytic activation of trypsinogen5 is sufficient to induce cell death.

Because pIC-dependent pancreatitis in *Irf2*$^{-/-}$ mice can be prevented by inactivating IFNAR1 signaling (Fig. 1*E*), we focused on IFN signaling pathways to identify candidates that might trigger initial cell death following pIC treatment. Indeed,

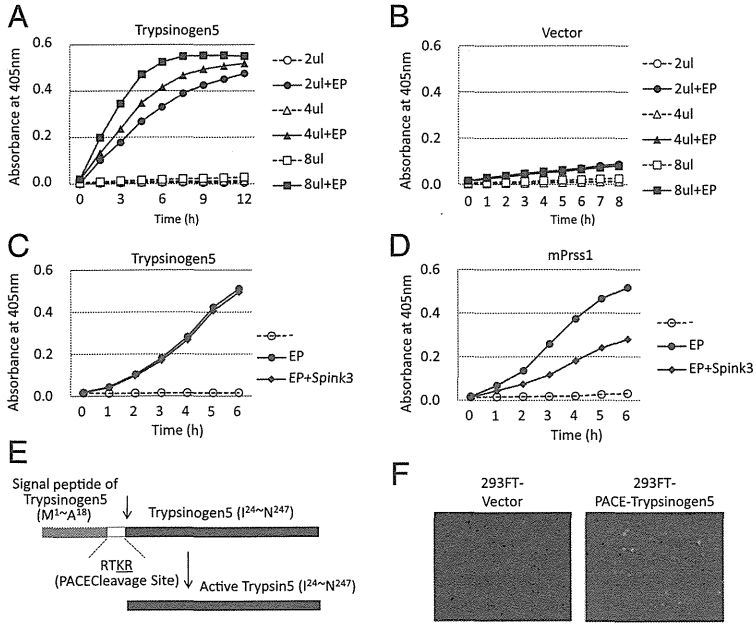

Fig. 4. Trypsinogen activity is activated by proteolytic cleavage. (*A* and *B*) A full-length mouse trypsinogen5 cDNA from the mouse pancreas was cloned into pcDNA3 (Invitrogen) and expressed in 293T cells. The indicated amounts of cell lysates (2–8 μL of 5 μg/μL lysates) were mixed with a trypsin-specific substrate (BioVision) in the presence or absence of added enteropeptidase. Tryptic activity was monitored by the amount of released pNA, measuring spectrophotometric units (A_{405}). (*C* and *D*) The effects of Spink3 were examined by adding cell lysates expressing Spink3, a major intrinsic trypsin inhibitor in mouse pancreas, to lysates expressing trypsinogen5 (*C*) or mouse Prss1 (*D*). (*E*) The DNA sequence encoding the activation peptide in the trypsinogen5 expression vector was replaced with sequences encoding a PACE cleavage site (-RTKR-) so that tryptic activity is activated by ubiquitously expressed PACE protease. (*F*) 293FT cells transfected with PACE-trypsinogen5 or control vector were stained with FITC-labeled annexin V to detect apoptosis.

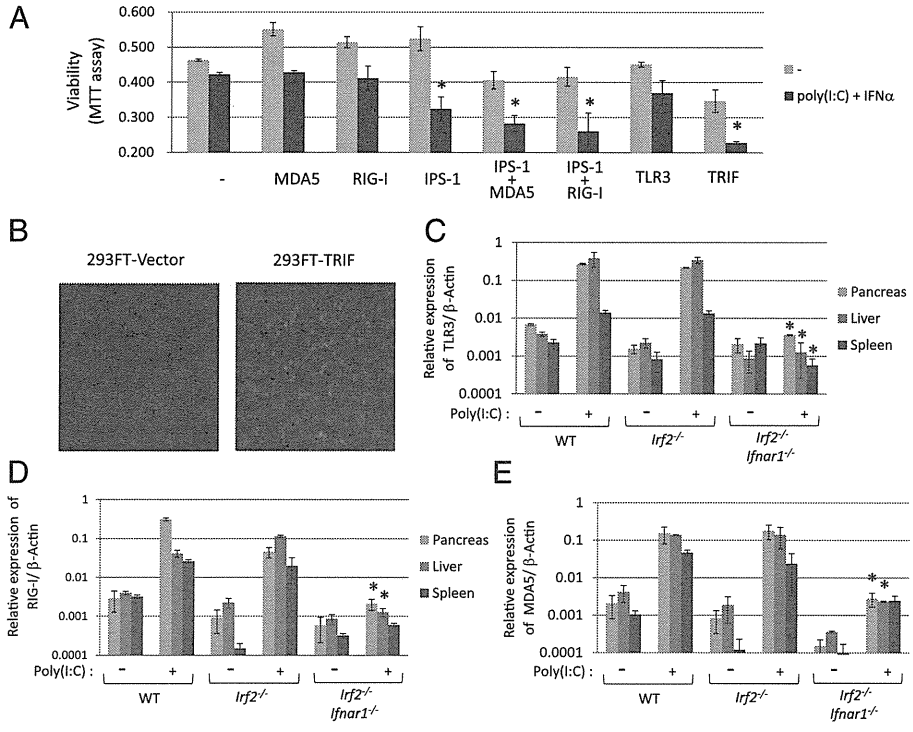

Fig. 5. Poly(I:C) and IFNα treatment induces cell death through different pathways. (*A*) Viabilities of 293FT cells transfected with the indicated expression plasmids in the presence or absence of pIC (5 μg/mL) and IFNα (50 ng/mL) for 44 h were quantified with the MTT assay. The values represent the average of at least three separate experiments, with SDs shown by error bars. TRIF and IPS-1 with MDA5 or RIG-I induced significant (*$P < 0.02$) cell death in response to pIC and IFNα. (*B*) 293FT cells transfected with TRIF expression vector or vector alone were stained with FITC-labeled annexin V to detect apoptosis. mRNA expression levels of TLR3 (*C*), RIG-I (*D*), and MDA5 (*E*) were measured using real-time PCR with (+) or without (–) i.p. pIC injection (250 μg). mRNAs prepared from pancreas, liver, and spleen of WT, *Irf2*$^{-/-}$, and *Irf2*$^{-/-}$*Ifnar1*$^{-/-}$ mice were converted into cDNA, and the amount of cDNA was determined by real-time PCR with the specific primers listed in *SI Materials and Methods*. The values represent the average of at least two mice, with SDs shown by error bars. *$P < 0.05$ versus *Irf2*$^{-/-}$ mice.

IRF1, *IRF7*, *MyD88*, *MDA5*, *RIG-I*, and *TLR3* gene expression were all up-regulated in the pancreas of pIC-*Irf2*$^{-/-}$ mice (Table S2). Because these proteins are associated with cell death pathways dependent on TRIF or IPS-1, we examined the effect of IRF2 loss on these well-characterized systems (21, 22). TRIF binds to receptor-interacting proteins and thereby activates caspase8 via FADD to induce cell death (21), whereas the IPS-1-dependent cell death pathway, which is triggered by MDA5 or RIG-I, is reported to activate caspase9 via the mitochondrial pathway dependent on Apaf-1 and cytochrome *c* (22). We confirmed that 293FT cells transfected with TRIF-expressing plasmid underwent apoptosis, as shown by staining with FITC-labeled annexin V (Fig. 5*B*). Next, we used the MTT viability assay to quantify the extent of cell death induced by IFN-related molecules in the presence or absence of pIC and IFNα. Exogenous overexpression of IPS-1 or TRIF significantly enhanced the death of pIC- and IFN-treated 293FT cells, and the death-inducing effects of MDA5 and RIG-I were enhanced by cotransfection with IPS-1 (Fig. 5*A*). These results suggest the existence of at least two pIC-dependent cell death pathways: one TLR3/TRIF-dependent and one RIG-I/MDA5/IPS-1-dependent.

We used real-time PCR to examine the induction of TLR3, RIG-I, and MDA5 mRNAs in pIC-treated WT, *Irf2*$^{-/-}$, and *Irf2*$^{-/-}$*Ifnar1*$^{-/-}$ mice. The levels of all three mRNAs were induced by nearly 100-fold in both pIC-WT and pIC-*Irf2*$^{-/-}$ mice, and these increases were abolished by deletion of IFNAR1 (Fig. 5 *C–E*). The IFN signal activation triggered by pIC is essential to initiate TLR3/TRIF- and RIG-I/MDA5/IPS-1-dependent acinar cell death, but is not sufficient to cause pancreatitis (Table S3). The elevation of trypsinogen5 expression mediated by abolishing IRF2 is also necessary for enhancing the cell death leading to lethal pancreatitis.

Activation Mechanisms of Mouse Trypsinogen5 and Human PRSS3. Trypsinogens (including trypsinogen5) can be activated in pancreatic acinar cells, or in other cells or tissues by enteropeptidase expressed in nonduodenal cells (23) such as in keratinocytes and oral carcinoma cells (24, 25). It is possible that keratinocyte-expressed enteropeptidase activates the trypsinogen5 expressed in skin (Fig. S3*A*), promoting age-dependent skin inflammation in *Irf2*$^{-/-}$ mice (4). Another possibility could be that proteases in addition to enteropeptidase can cleave pancreatic trypsinogen5. We have confirmed that cathepsin B, whose expression was elevated in *Irf2*$^{-/-}$ mice, can activate trypsinogen5 in vitro (Fig. S5*C*). The last possibility is that autocatalytic cleavage of trypsinogen, usually restricted under steady-state conditions, is accelerated in response to chemical stress or viral infection. Indeed, the autoactivation of trypsinogen is reportedly accelerated in low pH or by Ca^{2+} in vitro (26).

In conclusion, this study has identified important genes associated with IRF2 functions in mice. Our results suggest that IRF2 influences the expression of mouse trypsinogen5, whose human counterpart is PRSS3. Our data should therefore help to elucidate new IRF functions in humans.

Materials and Methods

Mice. *Irf1*$^{-/-}$ and *Irf2*$^{-/-}$ mice have been described (3). *IFNα/β receptor 1* (*Ifnar1*)$^{-/-}$ mice were purchased from B&K Universal (8). TRIF$^{-/-}$ mice have been described (9). *Irf2*$^{-/-}$*Ifnar1*$^{-/-}$, *Irf2*$^{-/-}$*Irf1*$^{-/-}$, and *Irf2*$^{-/-}$*Trif*$^{-/-}$ double mutant mice were generated by crossing *Irf2*$^{+/-}$ with *Ifnar1*$^{-/-}$, *Irf1*$^{-/-}$, and *Trif*$^{-/-}$ mice, respectively. All mice were maintained under specific pathogen-free conditions and used at 6–12 wk of age. All experiments were performed according to institutional guidelines.

Cells. Human embryonic kidney (HEK)293T and 293FT (Invitrogen) cells and HeLa cells were cultured in DMEM supplemented with 10% FBS. Mouse pancreatic acinar TGP49 cells were cultured in a 1:1 mixture of DMEM and Ham's F-12 medium supplemented with 10% FBS.

Histological Analysis. Pancreas tissues were fixed overnight in 10% formalin, embedded in paraffin, sectioned, and stained with hematoxylin (0.4%) and eosin (0.5%) for light microscopic analysis. For electron microscopic analysis, the tissues were fixed in 2.5% glutaraldehyde solution buffered to pH 7.4 with 0.1 M phosphate buffer for 4 h at 4 °C. Postfixation was performed with 2% osmium tetroxide solution buffered to pH 7.4 with the same buffer for 2 h at 4 °C, and they were embedded, sectioned, and doubly stained with uranyl acetate and lead nitrate.

Microarrays. Total RNAs from the pancreas of wild-type and *Irf2*$^{-/-}$ mice aged 6 wk, harvested 3 h after no injection or a peritoneal injection with 250 μg poly(I:C), were used in the array studies. The quality of the RNA was assessed with an Agilent 2100 Bioanalyzer, and samples of 100 ng total RNA were reverse-transcribed and then amplified by in vitro transcription according to Affymetrix standard protocols. The mouse Affymetrix GeneChip Mouse Gene 1.0 ST Array was used in all hybridizations. These arrays contain probes representing transcripts for 28,815 mouse gene entities. Microarray data were analyzed using Affymetrix Expression Console software and Gene Spring GX, whereas differentially expressed genes were identified with annotation.

Real-Time RT-PCR. Total RNA was prepared from tissues using the acid phenol-guanidinium thiocyanate method after immersing the tissues for more than overnight in RNAlater Solution (Ambion). Reverse transcription was conducted for 60 min at 46 °C from 200 ng of purified total RNA using SuperScript III (Invitrogen), followed by 45 cycles of PCR (15-s denaturation at 95 °C, 25-s annealing at 55 °C, and 15-s extension at 72 °C). An SYBR Green PCR Kit (Qiagen) was used to monitor the PCR products on a LightCycler 1.5 and real-time PCR detection system (Roche). Primers designed for the respective genes are listed in *SI Materials and Methods*.

Plasmid Constructs. cDNAs encoding human IRF5, IRF7, and IPS-1 were generated from total RNA prepared from 293T cells by RT-PCR using KOD-FX DNA polymerase (Toyobo). Human MDA5, RIG-I, and TLR3 cDNAs were generated from total RNA prepared from THP-1 (a human leukemia cell line) or HeLa cells by RT-PCR. Mouse Trypsinogen5, Prss1, and Spink3 cDNAs were made from total RNA prepared from WT mouse pancreas by PCR. All constructs generated by PCR were confirmed by DNA sequencing. The p*Trypsinogen5*-Luc reporter plasmid was constructed by inserting the promoter region (−1063 to +15) of the mouse *trypsinogen5* gene by PCR into the pGL2-Basic vector. A series of deletion mutants was prepared using proper restriction enzymes (NcoI at −833; SpeI at −579; ScaI at −386; PvuII at −216) and a specific primer for the −100 site. The promoter region (−216 to +15) of the mouse *trypsinogen5* gene was used to introduce point mutations into the ISREs. The point mutations of ISRE3 (−55 to −49, ATTGAAA→GTTTGCG), ISRE4 (−62 to −59, TTTC→CGCA), and ISRE5 (−84 to −78, AATGAAA→GATTGCG) were introduced by overlap PCR mutagenesis. All constructs generated by PCR were confirmed by DNA sequencing.

PACE-Trypsinogen5 was constructed by replacing the activation peptide (-NSDDK-) of mouse trypsinogen5 cDNA with the PACE recognition peptide (-RTKR-) by overlap PCR mutagenesis.

Luciferase Reporter Assay. 293T cells (1×10^5 per well) were plated in 24-well plates and transfected 24 h later with 200 ng of the firefly luciferase reporter plasmid p*Trypsinogen5*-Luc, using FuGENE6 (Roche), along with each expression vector (20 ng unless otherwise stated) as indicated. In all cases, cells were transfected with 20 ng pRL-TK (*thymidine kinase* promoter-driven Renilla luciferase reporter gene; Promega) to normalize the transfection efficiency. TGP49 cells (1×10^5 per well) were plated in 12-well plates and transfected 24 h later with 1 μg of the firefly luciferase reporter plasmid pTrypsinogen5-Luc using Lipofectamine 2000 (Invitrogen), along with each expression vector (100 ng unless otherwise stated) as indicated. In all cases, cells were transfected with 20 ng pRL-RSV (RSV promoter-driven Renilla luciferase reporter gene). At 26 h posttransfection, luciferase activity was determined with a dual luciferase assay system (Promega). Mouse IRF2-specific and control siRNAs were purchased from Santa Cruz Biotechnology.

Chromatin Immunoprecipitation. Nuclear extracts from TGP49 cells were subjected to DNA–protein cross-linking with 1% formaldehyde for 5 min. After extensive washing, the samples were suspended in 500 μL of 150 mM NaCl, 25 mM Tris (pH 7.5), 5 mM EDTA, 1% Triton X-100, 0.1% SDS, and 0.5% deoxycholate and sonicated. After centrifugation at 14,000 rpm for 10 min at 4 °C, the supernatants were immunoprecipitated with 0.5 μg anti-IRF2 antibody, or the corresponding IgG (Sigma) (as a control), and Protein A Sepharose4B Fast Flow beads. The amounts of precipitated DNA were quantified by PCR using a pair of mouse *Trypsinogen5* promoter-specific primers and *Angiotensinogen* exon2-specific primers (*SI Materials and Methods*).

Trypsin Activity Assay. Trypsin activity was monitored by the amount of released *p*-nitroanilide (pNA) from a specific substrate, measuring spectrophotometric units at 405 nm (A_{405}) (Trypsin Activity Assay Kit; BioVision). Cell lysates prepared at 48 h posttransfection of the indicated expression plasmids were used with or without enteropeptidase (light chain, porcine; GenScript).

Cell Death Assay. Pancreatic tissues were used in a TUNEL assay. Briefly, tissue sections were incubated with 20 μg/mL proteinase K for 20 min, followed by inhibition of endogenous peroxidase by incubation with 2% H_2O_2 for 7 min. TdT (GIBCO-BRL) and biotinylated dUTP (Roche) in TdT buffer [0.1 M potassium cacodylate (pH 7.2), 2 mM $CoCl_2$, 0.2 mM DTT] were added to the sections and incubated in a humid atmosphere at 37 °C for 90 min after immersion in TdT buffer. The reaction was terminated by transferring the slides to TB buffer (300 mM NaCl, 30 mM Na citrate) for 30 min. The sections were covered with 10% rabbit serum for 10 min and then with the avidin–biotin peroxidase complex for 30 min. Finally, 3,3′-diaminobenzidine (DAB) was used as the chromogen. To detect apoptotic cells, FITC-conjugated annexin V (BioVision) was used according to the manufacturer's instruction. An MTT (ICN) assay to assess living cells was performed according to the manufacturer's instruction.

ACKNOWLEDGMENTS. This work was supported by Grants-in-Aid from the Ministry of Education, Culture, Sports, Science and Technology of Japan (22659092) and by the Global Center of Excellence Program at Nagasaki University.

1. Savitsky D, Tamura T, Yanai H, Taniguchi T (2010) Regulation of immunity and oncogenesis by the IRF transcription factor family. *Cancer Immunol Immunother* 59:489–510.
2. Kawai T, Akira S (2011) Toll-like receptors and their crosstalk with other innate receptors in infection and immunity. *Immunity* 34:637–650.
3. Matsuyama T, et al. (1993) Targeted disruption of IRF-1 or IRF-2 results in abnormal type I IFN gene induction and aberrant lymphocyte development. *Cell* 75:83–97.
4. Hida S, et al. (2000) CD8(+) T cell-mediated skin disease in mice lacking IRF-2, the transcriptional attenuator of interferon-α/β signaling. *Immunity* 13:643–655.
5. Lampel M, Kern H-F (1977) Acute interstitial pancreatitis in the rat induced by excessive doses of a pancreatic secretagogue. *Virchows Arch A Pathol Anat Histol* 373:97–117.
6. Mashima H, et al. (2011) Interferon regulatory factor-2 regulates exocytosis mechanisms mediated by SNAREs in pancreatic acinar cells. *Gastroenterology* 141:1102–1113.
7. Gerke V, Creutz C-E, Moss S-E (2005) Annexins: Linking Ca^{2+} signalling to membrane dynamics. *Nat Rev Mol Cell Biol* 6:449–461.
8. Hwang SY, et al. (1995) A null mutation in the gene encoding a type I interferon receptor component eliminates antiproliferative and antiviral responses to interferons α and β and alters macrophage responses. *Proc Natl Acad Sci USA* 92:11284–11288.
9. Yamamoto M, et al. (2003) Role of adaptor TRIF in the MyD88-independent Toll-like receptor signaling pathway. *Science* 301:640–643.
10. Chen J-M, Férec C (2009) Chronic pancreatitis: Genetics and pathogenesis. *Annu Rev Genomics Hum Genet* 10:63–87.
11. Whitcomb D-C (2010) Genetic aspects of pancreatitis. *Annu Rev Med* 61:413–424.
12. Spicuglia S, Pekowska A, Zacarias-Cabeza J, Ferrier P (2010) Epigenetic control of Tcrb gene rearrangement. *Semin Immunol* 22:330–336.
13. Rowen L, et al. (2005) Interchromosomal segmental duplications explain the unusual structure of PRSS3, the gene for an inhibitor-resistant trypsinogen. *Mol Biol Evol* 22:1712–1720.
14. Figarella C, Miszczuk-Jamska B, Barrett A-J (1988) Possible lysosomal activation of pancreatic zymogens. Activation of both human trypsinogens by cathepsin B and spontaneous acid. Activation of human trypsinogen 1. *Biol Chem Hoppe Seyler* 369 (Suppl):293–298.
15. Halangk W, et al. (2000) Role of cathepsin B in intracellular trypsinogen activation and the onset of acute pancreatitis. *J Clin Invest* 106:773–781.
16. Meister T, et al. (2010) Missorting of cathepsin B into the secretory compartment of CI-MPR/IGFII-deficient mice does not induce spontaneous trypsinogen activation but leads to enhanced trypsin activity during experimental pancreatitis—without affecting disease severity. *J Physiol Pharmacol* 61:565–575.
17. Hashimoto D, et al. (2008) Involvement of autophagy in trypsinogen activation within the pancreatic acinar cells. *J Cell Biol* 181:1065–1072.
18. Negishi H, et al. (2005) Negative regulation of Toll-like-receptor signaling by IRF-4. *Proc Natl Acad Sci USA* 102:15989–15994.
19. Honda K, et al. (2005) Spatiotemporal regulation of MyD88-IRF-7 signalling for robust type-I interferon induction. *Nature* 434:1035–1040.
20. Ji B, Gaiser S, Chen X, Ernst S-A, Logsdon C-D (2009) Intracellular trypsin induces pancreatic acinar cell death but not NF-&kappaB activation. *J Biol Chem* 284: 17488–17498.
21. Kaiser W-J, Offermann M-K (2005) Apoptosis induced by the Toll-like receptor adaptor TRIF is dependent on its receptor interacting protein homotypic interaction motif. *J Immunol* 174:4942–4952.
22. Lei Y, et al. (2009) MAVS-mediated apoptosis and its inhibition by viral proteins. *PLoS One* 4:e5466.
23. Yahagi N, et al. (1996) Complementary DNA cloning and sequencing of rat enteropeptidase and tissue distribution of its mRNA. *Biochem Biophys Res Commun* 219:806–812.
24. Nakanishi J, Yamamoto M, Koyama J, Sato J, Hibino T (2010) Keratinocytes synthesize enteropeptidase and multiple forms of trypsinogen during terminal differentiation. *J Invest Dermatol* 130:944–952.
25. Vilen S-T, et al. (2008) Intracellular co-localization of trypsin-2 and matrix metalloprotease-9: Possible proteolytic cascade of trypsin-2, MMP-9 and enterokinase in carcinoma. *Exp Cell Res* 314:914–926.
26. Chen J-M, et al. (2003) Evolution of trypsinogen activation peptides. *Mol Biol Evol* 20: 1767–1777.

Periostin Facilitates Skin Sclerosis via PI3K/Akt Dependent Mechanism in a Mouse Model of Scleroderma

Lingli Yang[1,2], Satoshi Serada[2], Minoru Fujimoto[2], Mika Terao[1], Yorihisa Kotobuki[1,2], Shun Kitaba[1], Saki Matsui[1], Akira Kudo[3], Tetsuji Naka[2], Hiroyuki Murota[1]*, Ichiro Katayama[1]

1 Department of Dermatology, Osaka University Graduate School of Medicine, Osaka, Japan, **2** Laboratory for Immune Signal, National Institute of Biomedical Innovation, Osaka, Japan, **3** Department of Biological Information, Tokyo Institute of Technology, Yokohama, Japan

Abstract

Objective: Periostin, a novel matricellular protein, is recently reported to play a crucial role in tissue remodeling and is highly expressed under fibrotic conditions. This study was undertaken to assess the role of periostin in scleroderma.

Methods: Using skin from patients and healthy donors, the expression of periostin was assessed by immunohistochemistry and immunoblotting analyses. Furthermore, we investigated periostin$^{-/-}$ (PN$^{-/-}$) and wild-type (WT) mice to elucidate the role of periostin in scleroderma. To induce murine cutaneous sclerosis, mice were subcutaneously injected with bleomycin, while untreated control groups were injected with phosphate-buffered saline. Bleomycin-induced fibrotic changes were compared in PN$^{-/-}$ and WT mice by histological analysis as well as by measurements of profibrotic cytokine and extracellular matrix protein expression levels *in vivo* and *in vitro*. To determine the downstream pathway involved in periostin signaling, receptor neutralizing antibody and signal transduction inhibitors were used *in vitro*.

Results: Elevated expression of periostin was observed in the lesional skin of patients with scleroderma compared with healthy donors. Although WT mice showed marked cutaneous sclerosis with increased expression of periostin and increased numbers of myofibroblasts after bleomycin treatment, PN$^{-/-}$ mice showed resistance to these changes. *In vitro*, dermal fibroblasts from PN$^{-/-}$ mice showed reduced transcript expression of alpha smooth actin and procollagen type-I alpha 1 (Col1α1) induced by transforming growth factor beta 1 (TGFβ1). Furthermore, recombinant mouse periostin directly induced Col1α1 expression *in vitro*, and this effect was inhibited by blocking the αv integrin-mediated PI3K/Akt signaling either with anti-αv functional blocking antibody or with the PI3K/Akt kinase inhibitor LY294002.

Conclusion: Periostin plays an essential role in the pathogenesis of Bleomycin-induced scleroderma in mice. Periostin may represent a potential therapeutic target for human scleroderma.

Citation: Yang L, Serada S, Fujimoto M, Terao M, Kotobuki Y, et al. (2012) Periostin Facilitates Skin Sclerosis via PI3K/Akt Dependent Mechanism in a Mouse Model of Scleroderma. PLoS ONE 7(7): e41994. doi:10.1371/journal.pone.0041994

Editor: Alessandra Rossini, Università degli Studi di Milano, Italy

Received March 16, 2012; **Accepted** June 28, 2012; **Published** July 24, 2012

Funding: This study was supported by a grant-in-aid for the Program for Promotion of Fundamental Studies in Health Sciences of the National Institute of Biomedical Innovation and Grant-in-Aid from the Ministry of Health, Labour and Welfare of Japan. The funders had no role in study design, data collection and analysis, decision to publish, or preparation of the manuscript.

Competing Interests: The authors have declared that no competing interests exist.

* E-mail: h-murota@derma.med.osaka-u.ac.jp

Introduction

Scleroderma is a connective tissue disorder with unknown etiology. The disease is characterized by excessive deposition of collagen and other extracellular matrix (ECM) proteins, resulting in fibrosis of skin and other visceral organs [1]. To date, despite much effort, there is still no established treatment for fibrosis in scleroderma.

The ECM of the skin is composed not only of structural proteins such as collagen type-I but of many different proteins that modulate cellular behavior. The interactions among various ECM proteins provide molecular signals to resident cells including dermal fibroblasts and play essential roles in the maintenance and turnover of the ECM. At present, ECM proteins are considered as key players in the pathogenesis of scleroderma.

Among ECM proteins, the cytokine transforming growth factor β1 (TGFβ1) is regarded as a master regulator of the disease process in scleroderma, since it potently accelerates fibrosis in skin by inducing collagen production; various pro-fibrotic ECM proteins such as CCN2 (also known as a connective tissue growth factor or CTGF) are known to induce the transdifferentiation of fibroblasts to myofibroblasts [2,3]. Recently, a class of ECM proteins called matricellular proteins has attracted increasing attention in the field of scleroderma research. These proteins specifically regulate cell-matrix interactions and play critical roles in embryonic development as well as in tissue repair and fibrosis. Indeed, several matricellular proteins, including CCN2 [4], CCN1 (cysteine-rich protein 61) [5], and their cell-adhesive receptor, integrin β1 [6], have been shown to play roles in scleroderma, and such studies are still ongoing. Thus, investigations of the functions of ECM proteins and their signaling networks are urgently needed to elucidate the pathogenesis of scleroderma and develop new therapies.

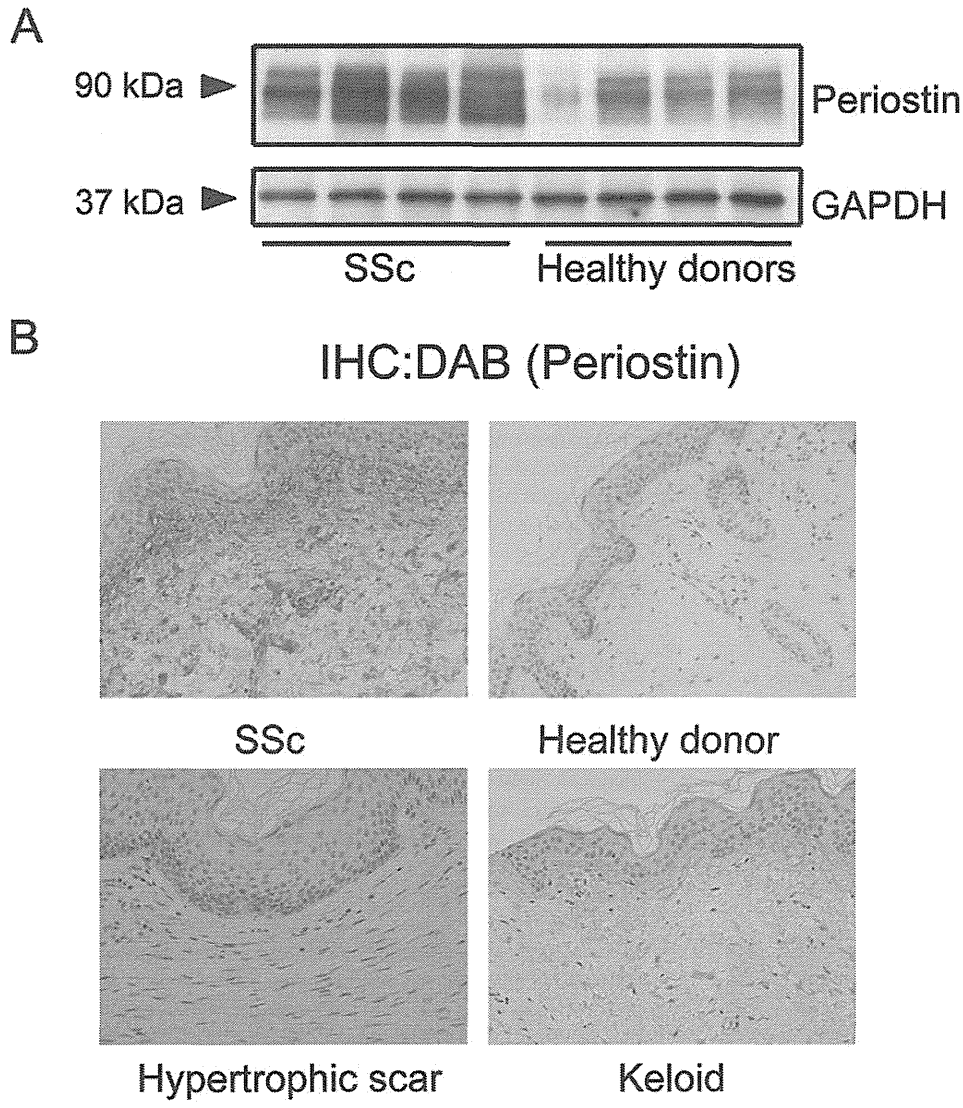

Figure 1. Periostin is overexpressed in lesional skin derived from patients with systemic scleroderma (SSc). A, Western blotting analysis for periostin using protein extracts from the skin of SSc patients and healthy donors. B, Representative immunohistochemistry of skin sections of SSc patients, healthy donors, hypertrophic scar and keloid patients. Slides were stained with anti-periostin antibodies (original magnification, ×100).
doi:10.1371/journal.pone.0041994.g001

To investigate the involvement of matricellular proteins in the pathogenesis of scleroderma, we focused on a novel matricellular protein, periostin, a 90-kDa, secreted, homophilic cell adhesion protein. Despite being first identified 15 years ago as osteoblast-specific factor-2 [7], periostin is now classified as a matricellular protein, because it is expressed in many collagen-rich tissues and possesses important biological functions in the ECM [8]. Periostin can bind to collagen during fibrillogenesis, thus affecting the diameter of collagen fibers and the extent of cross-linking [9,10]. Periostin also binds to other ECM proteins, including fibronectin and tenascin-C, thereby organizing the ECM architecture. Like other matricellular proteins, such as CCN1, CCN2, and CCN3 (capable of interacting with αv, β3, and β1 integrins) [11], periostin serves as a ligand for integrins αv, β1, β3, β4, and β5 [12–14]. Such signals can mediate cell adhesion to the ECM and may regulate certain cellular behaviors, including intracellular signaling, proliferation, and differentiation [15].

Analysis on periostin$^{-/-}$ (PN$^{-/-}$) mice revealed that this protein plays a pivotal role in the development of heart, bones, and teeth [16]. Approximately 14% of PN$^{-/-}$ mice die postnatally prior to weaning [17], suggesting a role of periostin in the development of these tissues. In adults, periostin is prominently upregulated during ECM remodeling and fibrosis. The major producers of periostin are fibroblasts [18,19], and its expression is induced by various factors, including TGFβ1, interleukin (IL) 4, and IL13 [19,20]. The prominent expression of periostin has been detected during a number of remodeling processes, including myocardial infarction [21], wound repair [8,22–24], fibrotic scar formation [25], sub-epithelial fibrosis in bronchial asthma [20], and bone marrow fibrosis [26]. Studies of PN$^{-/-}$ mice with experimentally induced diseases have further confirmed that periostin, in many cases, is profoundly involved in the progression of tissue fibrosis [17,27–29]. However, in a model of bronchial asthma, PN$^{-/-}$ mice developed peribronchial fibrosis equivalent

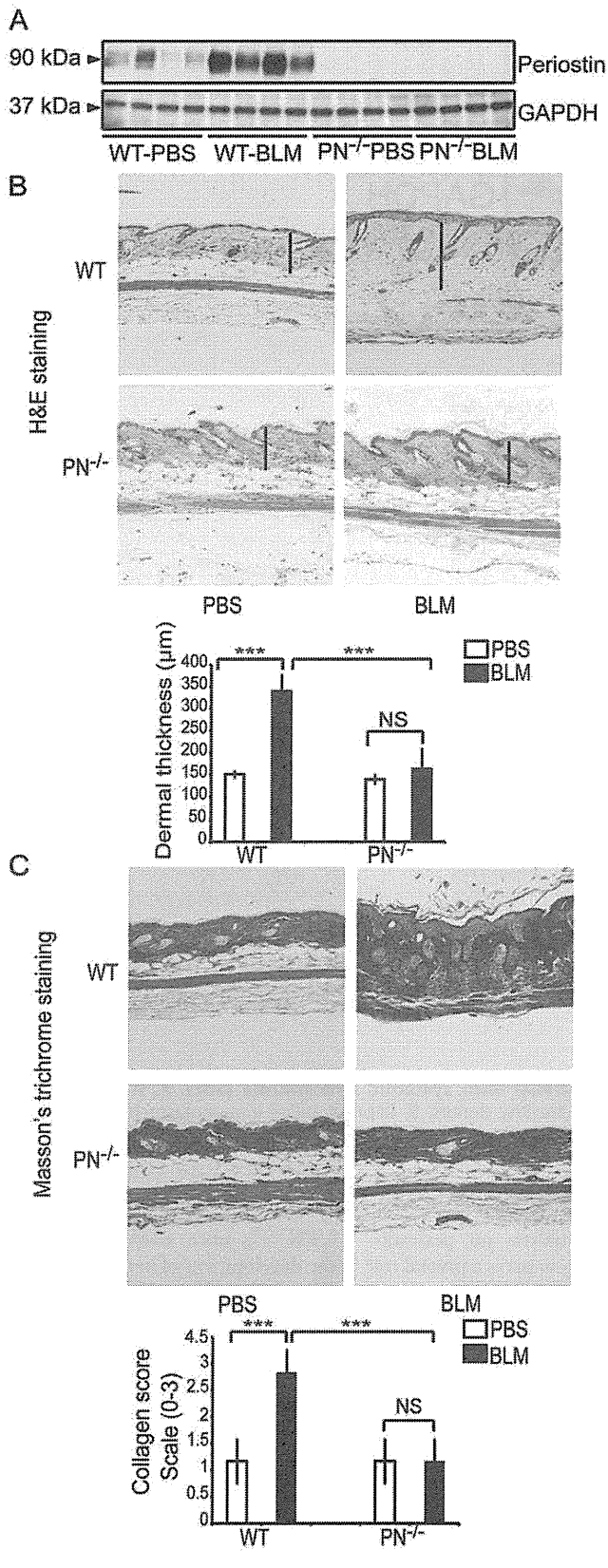

Figure 2. Periostin gene knockout ($PN^{-/-}$) mice are resistant to BLM-induced cutaneous sclerosis as assessed by dermal thickness and collagen deposition. A, Western blotting analysis for periostin in skin extracts from WT and $PN^{-/-}$ mice, which were treated with BLM or PBS. B, H&E staining of skin samples from WT and $PN^{-/-}$ mice (original magnification, ×100). Dermal thickness is shown as the black bar in the lower panel and was measured as described in the Materials and Methods. C, Masson's trichrome staining of skin samples from WT and $PN^{-/-}$ mice (original magnification, ×100). Collagen fibers were stained blue. Collagen deposition was scored on a scale of 0–3 as described in the Materials and Methods and is shown in the lower panel. For all assays, 10 mice from each group were analyzed. Values in B and C are shown as the mean ± SD. NS, no significance; ***, $p<0.01$.
doi:10.1371/journal.pone.0041994.g002

to WT mice [30], suggesting that periostin plays a limited role or is dispensable in certain conditions of fibrosis.

At present, it is unclear whether periostin is upregulated in the fibrotic lesions of scleroderma or plays a role in its pathology. In the present study, we analyzed periostin expression in skin samples from patients with systemic scleroderma, and the role of periostin in this disease, using $PN^{-/-}$ mice in a murine model of bleomycin (BLM)-induced scleroderma that exhibits defined cutaneous sclerosis that mimics human scleroderma [31].

Results

Periostin is Overexpressed in Lesional Skin of Patients with Scleroderma

To assess the involvement of periostin in the pathogenesis of scleroderma, we first compared the expression of periostin in sclerotic skin lesions from scleroderma patients and skin from identical areas of healthy donors. Based on western blotting analysis and immunohistochemical staining, periostin expression was markedly elevated in lesional skin from scleroderma patients compared with skin from healthy donors (Figure 1A and 1B). In addition, the distribution pattern of periostin in normal and fibrotic skin tissue appeared to be very different. In normal skin sections, periostin was faintly detectable in the upper dermis. In contrast, in scleroderma lesional skin, more intense staining for periostin was observed in the surrounding ECM throughout the dermis (Figure 1B). Furthermore, we examined periostin expression in the lesional skin from patients with other skin fibrotic diseases (keloid and hypertrophic scar), and found that periostin appeared to be expressed more strongly in lesional skin tissue of scleroderma than in those of keloid and hypertrophic scar (Figure 1B).

Periostin Gene Knockout Results in Reduced Symptoms of BLM-induced Cutaneous Sclerosis in Mice

Given these results above, it was logical to ask whether periostin plays an essential role in the pathophysiology of scleroderma or whether the altered expression of periostin is secondary to the disease process. To resolve this issue, we assessed the role of periostin in BLM-induced murine scleroderma using $PN^{-/-}$ mice [27]. To induce cutaneous sclerosis, we subcutaneously injected mice with BLM or PBS for four consecutive weeks, which has been widely used as an animal model of scleroderma [31]. Skin samples were collected one day after the final injection. To evaluate whether periostin is overexpressed in mice with BLM-induced scleroderma, the proteins extracted from mouse skin were subjected to western blotting analysis (Figure 2A). Indeed, periostin was strongly expressed in BLM-induced sclerotic skin of WT mice compared to skin samples from control PBS-treated mice. Antibody specificity was confirmed by the absence of a corresponding band in samples from $PN^{-/-}$ mice. These results agree with the supposition that elevated expression of periostin is closely linked to the pathogenesis of scleroderma.

Next, histological examinations of mouse skin sections using H&E staining (Figure 2B) were performed. As previously reported in this mouse model [32], a striking increase in dermal thickness and an apparent decrease in the amount of subcutaneous fat tissue (Figure 2B) were observed in WT mice injected with BLM. In contrast, $PN^{-/-}$ mice showed minimal dermal thickening (Figure 2B). WT mice showed a statistically significant increase of 220% ±33% in dermal thickness following BLM treatment ($p<0.01$), whereas, $PN^{-/-}$ mice did not develop apparent dermal thickening (Figure 2B, bar graph, lower panel).

Masson's trichrome staining, which stains collagen fibers blue, was performed to examine the increase of collagen fibers in BLM-treated mice (Figure 2C). WT BLM-treated mice displayed substantial thickening of the dermis with a robust deposition of collagen fibers that replaced the subcutaneous fat. These changes were markedly attenuated in BLM-treated $PN^{-/-}$ mice. Assessment using a four-point (grade 0–3) collagen deposition scoring system confirmed that the difference between $PN^{-/-}$ mice and WT mice was significant (Figure 2C, bar graph, lower panel).

Collectively, these results demonstrate that $PN^{-/-}$ mice display markedly reduced symptoms of BLM-induced cutaneous sclerosis, indicating that periostin is required for the development of BLM-induced cutaneous sclerosis.

Expression of Fibrogenic Cytokines and ECM Proteins in BLM-treated Mice Skin

Next, we assessed the expression of the main fibrogenic cytokines, TGFβ1 and CCN2 (also called CTGF), by real-time quantitative PCR. The expression of TGFβ1 and CCN2 (CTGF) mRNA after BLM treatment (Figure 3A and 3B) was increased in both WT and $PN^{-/-}$ mice, suggesting that the fibrotic process was initiated similarly in both $PN^{-/-}$ and WT mice. We then assessed the mRNA levels of Col1α1, a major component of dermal collagen fibers in these mice. Col1α1 mRNA levels were increased (536±76%) in WT mice skin after BLM treatment ($p<0.01$), but unexpectedly, not in BLM-treated $PN^{-/-}$ mice (Figure 3C). Thus, while periostin is known to regulate collagen assembly [10], these data suggest that periostin in BLM-induced scleroderma is critical for excessive collagen synthesis.

Periostin is Required for Myofibroblast Differentiation *in vivo*

It is widely accepted that α-SMA-expressing myofibroblasts, which are induced by fibrogenic cytokines, play key roles in collagen synthesis during the development of scleroderma [33]. To determine whether periostin is required for myofibroblast differentiation in this model, histoimmunohistochemistry for α-SMA (the most widely used myofibroblast marker) was performed on skin derived from WT and $PN^{-/-}$ mice with BLM or after PBS treatment (Figure 4A). $\alpha\text{-SMA}^+$ cells were increased in the dermis of skin sections from BLM-treated WT mice compared with skin from PBS-treated WT mice (Figure 4A). In contrast, $\alpha\text{-SMA}^+$ cells were not increased in BLM-treated $PN^{-/-}$ mice (Figure 4A). To detect myofibroblasts more specifically, double-labeling histoimmunofluorescence staining for anti-α-SMA and anti-CD34 (a representative vascular endothelial maker) were further performed (Figure 4B). Nonvascular α-SMA-positive CD34-negative spindle-shaped cells ($\alpha\text{-SMA}^+$ and $CD34^-$ cells), which indicate myofibroblasts, increased in the dermis of WT mice with statistical significance ($p<0.01$) but not in $PN^{-/-}$ mice (Figure 4C) after BLM treatment.

Supporting these data, western blotting analysis revealed an increase in the expression of α-SMA in skin derived from BLM-treated WT mice, but not $PN^{-/-}$ mice, compared with PBS-treated WT mice (Figure 4D). These results suggest that periostin is required for myofibroblast development in this scleroderma model.

Periostin is Required for TGFβ1-induced Myofibroblast Differentiation *in vitro*

TGFβ1 is the most potent inducer of myofibroblast differentiation in fibrosis [34]. To investigate the mechanism of action of periostin in myofibroblast generation, we isolated mouse dermal fibroblasts from WT and $PN^{-/-}$ mice and stimulated these cells with TGFβ1 *in vitro*. The induction of α-SMA at 2 hrs after TGFβ1 stimulation appeared similar between WT and $PN^{-/-}$ fibroblasts. However, after longer periods of stimulation (12 hrs, 24 hrs), α-SMA expression levels in $PN^{-/}$

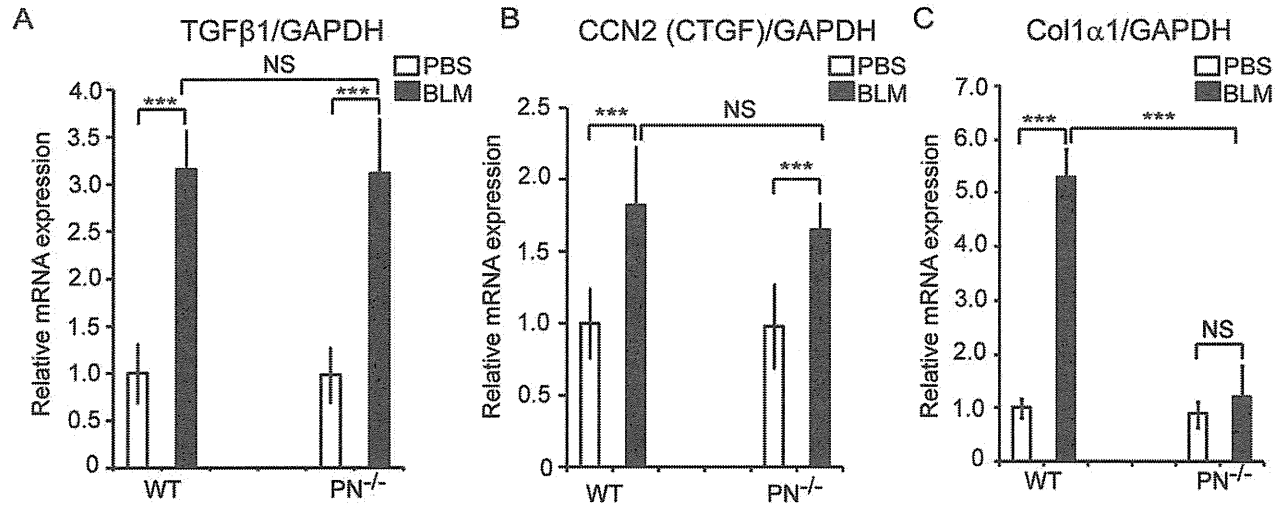

Figure 3. The expression of fibrogenic cytokines (TGFβ1 and CCN2/CTGF) and collagen type I in BLM-treated mouse skin. Real-time quantitative PCR analysis was performed to determine mRNA levels of TGFβ1 (A), CCN2 (CTGF) (B), and Col1α1 (C) in mouse skin of WT and $PN^{-/-}$ mice. Values were normalized to GAPDH levels and expressed as relative mRNA levels compared with PBS-treated WT mice. Values are shown as the mean ± SD. NS, no significance; ***, $p<0.01$.
doi:10.1371/journal.pone.0041994.g003

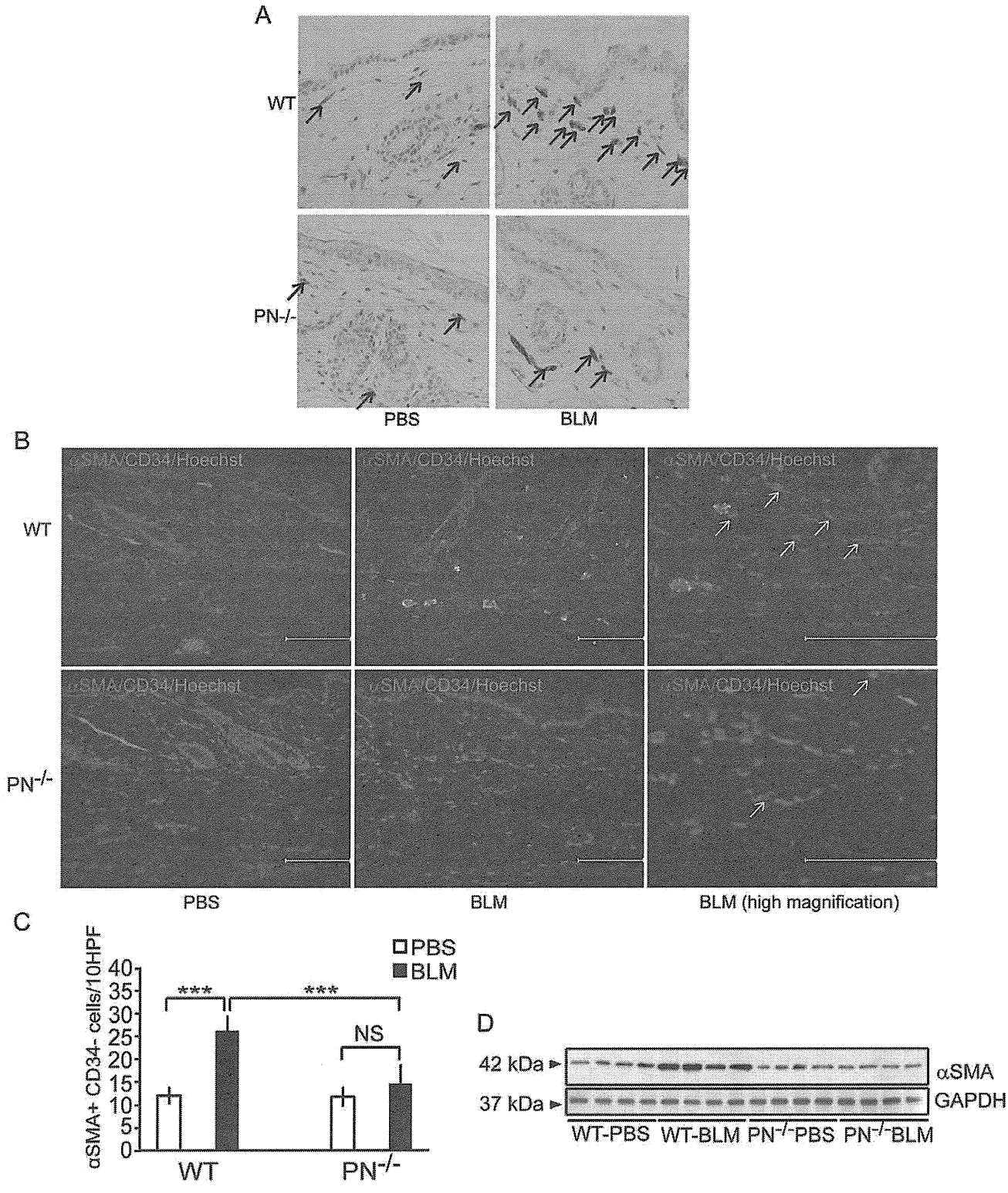

Figure 4. Periostin is required for dermal myofibroblast development in BLM-treated mice *in vivo*. A, Representative skin sections from WT and $PN^{-/-}$ mice, stained by immunohistochemistry with anti-α-SMA antibody (original magnification, ×400). α-SMA-positive myofibroblasts are indicated by arrows. B, Representative skin sections from WT and $PN^{-/-}$ mice, doubly stained by immunofluorescence for anti-α-SMA (red) and anti-CD34 (green). $\alpha\text{-SMA}^{+}$ $CD34^{-}$ spindle-shaped myofibroblasts are indicated by arrows. Scale bar = 100 μm. Nucleic staining: Hoechst 33342 (blue). C, The number of myofibroblasts per 10 hyper power microscopic fields is shown in the histogram. D, Western blotting analysis of protein extracted from WT and $PN^{-/-}$ mice skin tissues. For all assays, 10 mice from each group were analyzed. Values in C are shown as the mean ± SD. NS, no significance; ***, $p<0.01$.

doi:10.1371/journal.pone.0041994.g004

$^{-}$ fibroblasts were significantly lower than those in WT fibroblasts ($P<0.01$) (Figure 5A). Western blotting analysis, using protein samples extracted from cultured fibroblasts 24 hrs after TGFβ1 stimulation, confirmed that α-SMA protein levels were strongly induced in WT fibroblasts but not in $PN^{-/-}$ fibroblasts (Figure 5B). In addition, WT fibroblasts stimulated with TGFβ1 for more than 12 hrs could upregulate periostin at the protein levels (Figure S2B). These results raise the possibility that periostin protein induced by TGFβ1 may directly or indirectly mediate α-SMA expression in fibroblasts. Therefore, we next stimulated cultured WT dermal fibroblasts with different concentrations of rmPeriostin alone or in combination with TGFβ1 for two hours. While neither α-SMA transcript expression (Figure 5C) nor α-SMA protein expression (Figure 5D) was increased by rmPeriostin stimulation alone, the α-SMA expression level was synergistically enhanced by the combined stimulation of rmPeriostin with TGFβ1, compared to that with TGFβ1 stimulation alone (Figure 5C and 5D). These results suggest that periostin can enhance α-SMA expression in fibroblasts, not by acting alone but by cooperating with TGFβ1.

Periostin Upregulates Col1α1 Expression via the αv-integrin Mediated Phosphoinositide 3 Kinase (PI3K)/Akt Signaling Pathway *in vitro*

TGFβ1 is also known as a major inducer of collagen synthesis. We therefore investigated Col1α1 transcript levels in WT and $PN^{-/-}$ fibroblasts when they were stimulated with TGFβ1. Similar to the results of α-SMA expression, Col1α1 expression in $PN^{-/-}$ fibroblasts became to be significantly lower than WT fibroblasts after 12 hours of stimulation (Figure 6A). This result suggests that periostin may play a role in the Col1α1 expression.

To elucidate whether periostin directly enhances collagen synthesis, the effects of periostin on Col1α1 expression were also examined in cultured WT dermal fibroblasts. Interestingly, Col1α1 expression was induced two hours after stimulation with rmPeriostin alone in a dose-dependent manner (Figure 6B). In addition, Col1α1 expression level was further enhanced by the combined stimulation of rmPeriostin and TGFβ1, compared to TGFβ1 or rmPeriostin stimulation alone (Figure 6B), indicating the additive effect of rmPeriostin on TGFβ1-induced collagen induction.

Finally, to further clarify the signaling pathway by which periostin regulates Col1α1 expression, receptor neutralizing and kinase inhibition analyses were performed. After identification the optimal concentration of each inhibitor by a series dilution prior to the initiation of experiments, mouse dermal fibroblasts were pre-treated for two hours with or without various inhibitors at the identified concentrations: a neutralizing antibody against the known periostin receptor of αv-integrin (anti-αv integrin Ab), a tyrosine kinase inhibitor (genistein), a PI3K/Akt kinase inhibitor (LY294002), a mitogen-activated protein (MAP) kinase inhibitor (PD98095), an extracellular signal-related kinase (ERK) inhibitor (U0126), a p38 MAP kinase inhibitor (SB203580), or mammalian target of rapamycin (mTOR) inhibitors (temsirolimus and rapamycin). Fibroblasts were then stimulated with rmPeriostin for two hours to measure Col1α1 mRNA levels by real-time quantitative PCR (Figure 6C). Among these pharmacological inhibitors, only the addition of

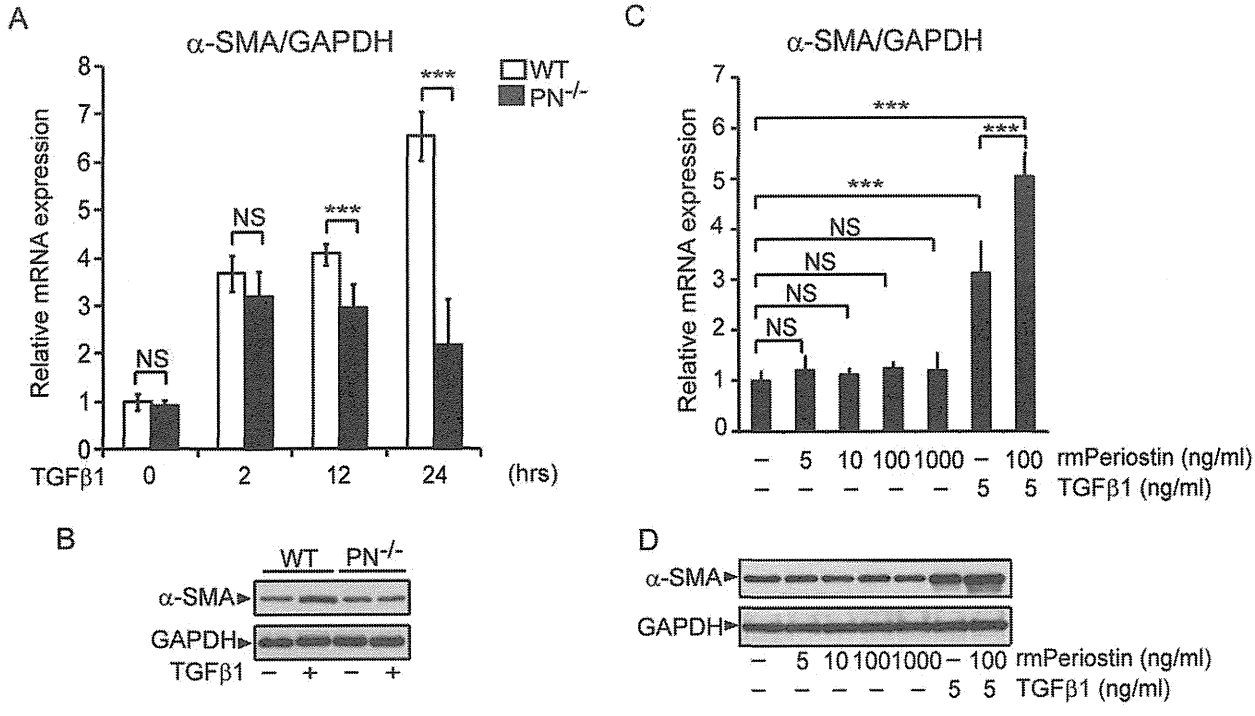

Figure 5. Periostin is required for TGFβ1-induced myofibroblast differentiation *in vitro*. A, Real-time quantitative PCR was performed to determine relative mRNA levels of α-SMA in cultured mouse dermal fibroblasts after TGFβ1 stimulation at the indicated times. B, Western blotting analysis for α-SMA with protein extracted from the indicated mouse dermal fibroblasts after TGFβ1 stimulation. C, Relative mRNA levels of α-SMA in cultured WT mouse dermal fibroblasts after the indicated stimulation. D, Western blotting analysis for α-SMA with protein extracted from WT mouse dermal fibroblasts after the indicated stimulation. Values in A and C were normalized to GAPDH levels and expressed as relative mRNA levels compared with WT mice fibroblasts (A) or WT dermal fibroblasts without stimulation (C). Values in A and C are shown as the mean ± SD. NS, no significance; ***, $p<0.01$.
doi:10.1371/journal.pone.0041994.g005

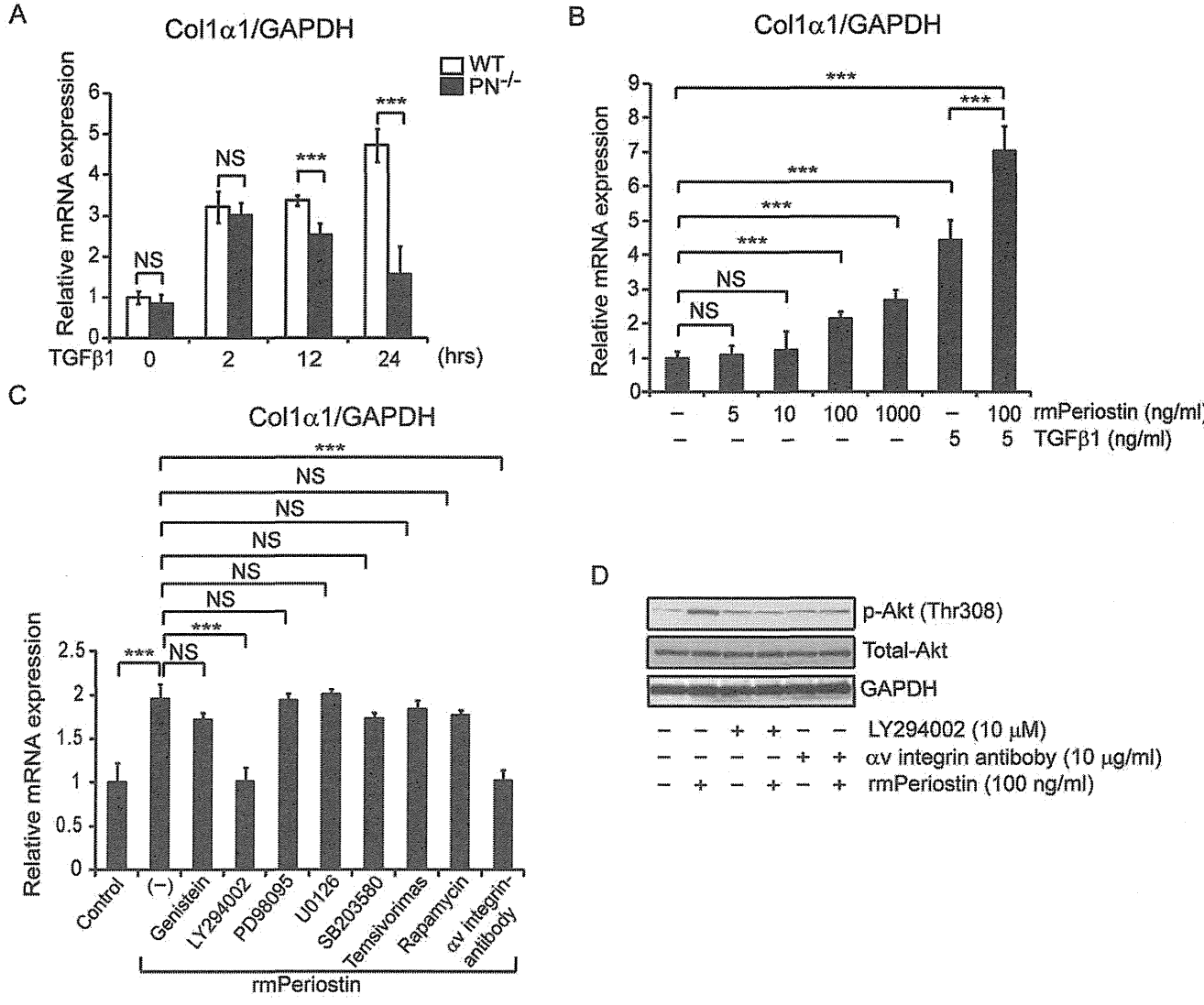

Figure 6. Periostin upregulates the expression of Col1α1 via αv-integrin mediated-PI3K/Akt signaling pathway *in vitro*. A, Real-time quantitative PCR was performed to determine relative mRNA levels of Col1α1 in cultured dermal fibroblasts from WT and $PN^{-/-}$ mice after TGFβ1 stimulation at the indicated times. B, Relative mRNA levels of Col1α1 in WT mouse dermal fibroblasts with the indicated stimulation. C, Relative mRNA levels of Col1α1 in cultured WT mouse dermal fibroblasts treated with rmPeriostin in the presence or absence of the indicated neutralizing antibody or kinase inhibitors. D, Phosphorylation of Akt in cultured WT mouse dermal fibroblasts treated with or without rmPeriostin in the presence or absence of LY294002 or anti-αv neutralizing antibody. Values in A, B, and C were normalized to GAPDH levels and expressed as relative mRNA levels compared with WT mice fibroblasts (A) or WT dermal fibroblasts without stimulation (B and C). NS, no significance; ***, $p<0.01$.
doi:10.1371/journal.pone.0041994.g006

LY294002 (10 μM) and anti-αv integrin Ab (10 μg/ml) abrogated periostin-induced upregulation of Col1α1 expression. In addition, rmPeriostin promptly activated Akt (Thr308) in WT mouse dermal fibroblasts (Figure 6D), implying the direct activation of the PI3K/Akt pathway by rmPeriostin. We also confirmed that the nontoxic concentration of LY294002 and anti-αv integrin Ab efficiently blocked Akt phosphorylation in fibroblasts treated with rmPeriostin (Figure 6D). Thus, periostin appears, at least in part, to directly increase Col1α1 expression in murine scleroderma via the αv integrin-mediated PI3K/Akt pathway.

Discussion

Matricellular proteins are ECM proteins that modulate cell-matrix interactions as well as cellular functions. They are highly expressed in injured and remodeled tissues and during embryonic development, and have been implicated in the pathophysiology of various fibrotic conditions. Like other matricellular proteins, periostin is thought to play a fundamental role in tissue development and remodeling [10,27,35]. Using $PN^{-/-}$ mice, the importance of periostin in various fibrotic conditions has been uncovered. However, it is still unknown whether periostin is involved in scleroderma. Our study is the first to assess the role of periostin in scleroderma.

As expected, we show herein the enhanced expression of periostin in lesional skin from patients with scleroderma and in BLM-induced sclerotic mouse skin, compared with hypertrophic scar, keloid, normal skin and PBS-treated mouse skin. These observations support the notion that periostin is involved in the process of skin fibrosis.

$PN^{-/-}$ mice were used to examine the contribution of periostin in the pathogenesis of scleroderma. The results of histological analysis showed that before the subcutaneous injection of BLM, there were no significant differences in dermal thickness or collagen production between WT and $PN^{-/-}$ mice. However, in the BLM-induced mouse scleroderma model, a reduced sclerotic response was shown in the skin of $PN^{-/-}$ mice, suggesting that periostin is critically involved in the pathogenesis of scleroderma.

The enhanced generation of α-SMA-positive myofibroblasts is determined to be a hallmark of and an essential process for scleroderma [33]. In the present study, BLM-induced myofibroblast formation was distinctly impaired in $PN^{-/-}$ mice. A similar reduction in the development of α-SMA-positive myofibroblasts has been observed previously in $PN^{-/-}$ mice subjected to various pathogenic conditions such as myocardial infarction [17,36], wound healing [37] and tumor engraftment [27]. These observations collectively indicate the important role of periostin in myofibroblast development *in vivo*.

One possible mechanism by which periostin can increase myofibroblast number is the promotion of myofibroblast recruitment through the αv-integrin pathway [17,21]. It is also well known that myofibroblast differentiation is critically regulated by TGFβ1 and TGFβ1-induced matricellular proteins such as CCN2 and fibronectin [4,38,39]. In the present study, myofibroblast differentiation induced by TGFβ1 *in vitro* was attenuated in $PN^{-/-}$ fibroblasts (Figure 5A and 5B), although we found no impairment of cell viabilities in $PN^{-/-}$ fibroblasts during culture (Figure S1 and Text S1). Moreover, this impairment in $PN^{-/-}$ fibroblasts was rescued by the addition of rmPeriostin *in vitro* (Figure S3A). Interestingly, however, we found that periostin stimulation alone did not induce α-SMA expression in WT fibroblasts, but the TGFβ1-induced α-SMA expression could be enhanced in combination with rmPeriostin. Similar to our findings, a previous study showed that periostin is required for embryonic fibroblasts to respond properly to TGFβ1 [40]. Thus, it appears that periostin likely plays a critical role as a co-factor that augments TGFβ1-induced α-SMA expression. This action of periostin is reminiscent of other matricellular proteins such as CCN2 in facilitating TGFβ1 action [38]. Thus, periostin, in cooperation with other TGFβ1-induced matricellular proteins, may provide integrated extracellular signals for a proper TGFβ1 response. In addition, periostin may also augment TGFβ1 activity *via* the activation of latent TGFβ1, as suggested by a previous study on airway epithelial cells [41].

Our findings also suggest that periostin directly contributes to excessive collagen synthesis in scleroderma. Previously, in various disease models utilizing $PN^{-/-}$ mice, reductions in collagen accumulation, similar to our observations, were reported [17,27–29]. However, it is unknown whether periostin directly regulates collagen synthesis. In this study, both $PN^{-/-}$ mice upon bleomycin injection *in vivo* and $PN^{-/-}$ fibroblasts stimulated with TGFβ1 *in vitro* exhibited reduced Col1α1 mRNA production. Furthermore, rmPeriostin induced Col1α1 mRNA expression in dermal fibroblasts *in vitro*. These effects of periostin are presumably direct and mediated *via* the αv-integrin mediated-PI3K/Akt pathway because 1) rmPeriostin can induce a prompt activation of Akt in fibroblasts and 2) Col1α1 induction was abrogated by αv-integrin neutralization or PI3K inhibition. It is known that periostin can bind to several types of integrins (e.g., αvβ3, αvβ5, and αvβ4), which act as receptors that activate downstream signaling pathways including PI3K/Akt [13]. Our findings also raise the intriguing possibility that TGFβ1-induced Col1α1 expression, unlike α-SMA expression, is mediated by the action of periostin. These observations of periostin differ from those obtained using $CCN2^{-/-}$ fibroblasts, in that Col1α1 production normally increases after TGFβ1 stimulation [4]. It is tempting to speculate that Col1α1 production in $CCN2^{-/-}$ fibroblasts might be compensated by the effects of TGFβ1-induced periostin. Thus, we assume that periostin, upon induction by TGFβ1, not only acts as a co-factor of TGFβ1 activity, but also, at least in part, directly mediates part of the TGFβ1 response.

Our time-course experiments *in vitro* revealed that mRNA levels of α-SMA and Col1α1 were similar between WT and $PN^{-/-}$ fibroblasts at the early phase of TGFβ1 stimulation (0 hrs, 2 hrs), but became prominently lower in $PN^{-/-}$ fibroblasts than that in WT fibroblasts after longer incubation with TGFβ1 (12 hrs, 24 hrs) ($P<0.01$) (Figure 5A and 6A). This difference at late phase can be explained by de novo periostin secretion, which is induced by TGFβ1 in WT fibroblasts. Indeed, as reported previously [19], periostin was strongly induced in fibroblasts by TGFβ1 in a dose-dependent manner (Figure S2A). Moreover, the protein synthesis and secretion of periostin was undetectable at 2 hrs but became detectable after 12 hrs of stimulation (Figure S2B). Notably, TGFβ1-induced expression of α-SMA and Col1α1 in $PN^{-/-}$ fibroblasts could be rescued by addition of rmPeriostin to the culture media (Figure S3A and S3B). Upon these results described above, periostin, induced by TGFβ1 in fibroblasts, is likely involved in fibrosis process of scleroderma, at least in part *via* enhancing α-SMA expression and mediating Col1α1 induction in these cells.

The unexpected data we encountered in the present study was that, in $PN^{-/-}$ fibroblasts, TGFβ1-induced α-SMA and Col1α1 mRNA levels were peaked at 2 hrs and slightly declined thereafter (Figure 5A and 6A). Because it is well known that the fibrotic effect of TGFβ1 is regulated by its negative feedback mechanisms, the absence of periostin may render these feedback mechanisms predominant. Furthermore, our preliminary data suggest that the expression of decorin, which is known as a potent inhibitor of TGFβ1/Smad signaling [42], is increased in $PN^{-/-}$ fibroblasts compared to WT cells (data not shown). Thus, periostin may accelerate the fibirotic action of TGFβ1 not only by increasing α-SMA and Col1α1 mRNA expression but also by counteracting against negative feedback signaling of TGFβ1. Further studies are underway to reveal the role of periostin in regulating negative-feedback signaling molecules such as decorin and Smad7 in TGFβ1 signaling.

It should be noted that periostin is reported to have a number of functions that may related to skin fibrosis. Similar to other matricellular proteins like thrombospondin-2 [41] and SPARC (secreted protein acidic and rich in cysteine, also known as osteonectin or BM-40) [42], periostin is known to be involved in collagen assembly [10]. Moreover, we recently reported that rmPeriostin can promote the proliferation of mouse dermal fibroblasts *in vitro* [24], at least in part *via* periostin-PI3K/Akt pathway. Additionally, according to recent evidence [29,43], periostin may also contribute to scleroderma *via* the regulation of the Notch1 signaling pathway, another important pathway in skin sclerosis [44–46].

It is generally known that fibrotic processes in skin are regulated by a complex network of matricellular proteins. Inhibition of just one matricellular protein can often disrupt the balance of this organized network and lead to exacerbation [43] or attenuation [4] [6,44] of skin fibrosis under pathogenic conditions. The present study is the first to show that periostin is one of these pivotal matricellular proteins that accelerates pathologic fibrosis in both BLM-induced skin sclerosis and human scleroderma. Our findings suggest that periostin promotes disease by enhancing myofibroblast differentiation and collagen synthesis via the augmentation